Structure, activity and function of a singing-CPG interneuron controlling cricket species-specific acoustic signaling

Abbreviated title: Species-specific singing-CPG

Pedro F. Jacob[1, 2, 3] and Berthold Hedwig[1]

[1]Department of Zoology, University of Cambridge, Downing Street, Cambridge, CB2 3EJ, United Kingdom; [2]Champalimaud Neuroscience Programme, Champalimaud Centre for the Unknown, Lisbon, Portugal; [3]Present Address: Centre for Neural Circuits and Behaviour, The University of Oxford, Tinsley Building, Mansfield Road, Oxford OX1 3SR, United Kingdom

Corresponding author: B. Hedwig: Department of Zoology, University of Cambridge, Downing Street, Cambridge, CB2 3EJ, United Kingdom. Telephone: ++44 1223 336603 / Fax: ++44 1223 336676 / E-mail: bh202@cam.ac.uk.

- Number of pages: 36 Number of figures: 9 Number of tables: 3
- Number of words: Abstract 170; Introduction 585; Discussion 1555

Acknowledgements

We are grateful to Gerald Pollack (McGill University) for providing *G. assimilis* and *G. rubens* eggs; and to Nathan Bailey (University of St. Andrews) and his team (Tony Ly, Suzanne Vardy, Peter Moran and Katherine Holmes) for eggs of *T. commodus* and *T. oceanicus*, which were used to establish the populations used in this study. We thank Nigel Hall for technical support in rearing the crickets. We thank Steve M. Rogers for comments on the manuscript. PFJ was supported by the Fundação para a Ciência e a Tecnologia, Portugal

(SFRH/BD/51901/2012) and the equipment used in this research was funded by the BBSRC (BB/G018723/1).

Conflict of interest

The authors declare no competing interest for this work.

Author Contributions

P.F.J. and B.H. conceptualized and designed the experiments. P.F.J. performed the experiments and analyzed the data. P.F.J. prepared the figures and drafted the manuscript. P.F.J. and B.H. revised and approved the final version of the manuscript.

Abstract

The evolution of species-specific song patterns is a driving force in the speciation of acoustic communicating insects. It must be closely linked to adaptations of the neuronal network controlling the underlying singing motor activity. What are the cellular and network properties that allow generating different songs? In five cricket species, we analyzed the structure and activity of the identified abdominal ascending opener interneuron, a homologous key component of the singing central pattern generator. The structure of the interneuron, based on the position of the cell body, ascending axon, dendritic arborization pattern, and dye-coupling is highly similar across species. The neuron's spike activity shows a tight coupling to the singing motor activity. In all species, current injection into the interneuron drives artificial song patterns, highlighting the key functional role of this neuron. However, the pattern of the membrane depolarization during singing, the fine dendritic and axonal ramifications and the number of dye-coupled neurons, indicate species-specific adaptations of the neuronal network, which might be closely linked to the evolution of species-specific singing.

Key words: singing-CPG, species-specific behavior, activity patterns, neuronal mechanisms, evolutionary neurobiology

Significance Statement: A fundamental question in evolutionary neuroscience is how species-specific behaviors arise in closely-related species. We demonstrate behavioral, neurophysiological and morphological evidence for homology of one key identified interneuron of the singing central pattern generator in five cricket species. Across species differences of this interneuron are also observed, which might be important to the generation of the species-specific song patterns. This work offers a comprehensive and detailed

comparative analysis addressing the neuronal basis of species-specific behavior.

Introduction

Behavioral changes in signaling for mate attraction and courtship are very important in speciation processes (Muller 1939; Kaneshiro 1980; Endler and Basolo 1998; Boughman 2002; Ritchie 2007). Changes in species-specific behavior can be achieved by altering the signal type e.g. converting between sound and vibration (ter Hofstede et al. 2015), modifications of peripheral structures, while keeping the motor patterns (Elsner and Wasser 1995; Vedenina et al. 2012), or adaptations at the level of the nervous system that lead to different motor patterns (Katz and Harris-Warrick 1999). Comparing identified neurons and network properties in closely related species that just differ in the motor patterns used to generate sexual communication signals (Arbas et al. 1991; Crews 1997; Katz and Harris-Warrick 1999; Ritchie 2007) provides the chance to gain insights into evolutionary specializations of neural circuits.

Two of the most impressive examples of species-specific motor patterns separating species occur in acoustically communicating insects on Hawaii, within the "picture-winged" *Drosophila* species group (Hoy et al. 1988; Hoikkala et al. 1989), and the crickets of the genus *Laupala* (Shaw 1996; Mendelson and Shaw 2002). In both groups sister species may be morphologically identical but the temporal patterns of the male song, closely linked to the female signal preferences, drove speciation (Hoikkala et al. 1994; Mendelson and Shaw 2005). The temporal structure of the signal patterns is under the control of the nervous system, by the activity of central pattern generators (CPGs; Capranica 1992; Chagnaud et al. 2011; Schöneich and Hedwig 2012). Recently the neuronal basis for the singing-CPG in *Drosophila* (Clyne and Miesenböck 2008; von Philipsborn et al. 2011, 2014, Shirangi et al. 2013, 2016, Ding et al. 2016) has been explored with genetic approaches. Crickets, however offer advantages given the detailed knowledge of the song circuitry and its electrophysiological properties (Bentley 1969; Hennig 1989, Kutsch and Huber 1989; 1990;

Schöneich et al. 2011; Schöneich and Hedwig 2012). Furthermore, the specific genetic tools in *Drosophila* that allow labelling of single neurons are for the most part limited to one species.

Crickets display species-specific song patterns, identical in their role as a far field communication signal to attract females. This supports the homology of the acoustic behavior in crickets (Alexander 1962; Otte 1992), offering the opportunity to identify and compare homologous neurons across species, in order to gain insights into the neural basis of signaling behavior and its species-specific neural specializations during evolution.

Male crickets sing by rhythmically opening and closing their front wings. This movement is generated by the activity of wing-opener and wing-closer muscles and motoneurons, their activity mirrors the species-specific pulse pattern in fictive singing (Kutsch and Huber 1989; Poulet and Hedwig 2003). Songs can be described by the carrier frequency and the pulse pattern. Within the temporal domain, each closing movement generates a short sound pulse, and in a song, these are organized in a species-specific manner in groups or sequences of pulses i.e. chirps and trills. Although the wing size and shape can affect sound production (Montealegre-Z. et al. 2011), these parameters are only weakly correlated with calling song structure (Blankers et al. 2017), pointing to the importance of the temporal parameters that are under control of the CPG.

Therefore, in order to understand how species-specific behaviors, arise in closely-related species we analyzed the abdominal ascending opener interneuron (A3-AO), an identified singing-CPG interneuron in bispotted field crickets, *Gryllus bimaculatus* (Schöneich and Hedwig 2011, 2012), across different species. We compared the structure, activity patterns and effect on singing motor pattern generation of A3-AO in five cricket species.

Material and methods

Animals

We used male crickets of *Gryllus bimaculatus* DeGeer; *Gryllus assimilis* Fabricius; *Gryllus rubens* Scudder; *Teleogryllus oceanicus* Le Guillou; and *Teleogryllus commodus* (Walker). Males were kept individually in plastic containers at 26-28ºC with a 12h light:dark cycle and were used from 7-21 days post-ecdysis. A mixture of protein-rich food, and water was provided ad-libitum. Experiments were carried out at 23-24ºC and complied with the principles of Laboratory Animal Care (ASAB Ethics Committee 1997).

Song recordings

Songs of individual males of each species were recorded for two to three nights with a PC microphone (Omni type; Maplin Electronics, Rotherham, UK) at a sampling rate of 48 kHz using Cool Edit 2000 software (Syntrillium Software Corporation, Phoenix, AZ, USA). See Jacob and Hedwig (2016) for details.

Dissection and pharmacological brain stimulation

Prior to experiments crickets were cooled down and were placed dorsal side up on a Plasticine ™ block by restraining all legs with metal clamps. The head was waxed to a metal holder and opened to access the brain. We accessed the central nervous system by a dorsal midline incision along the abdomen and thorax, peripheral nerves to the thoracic and abdominal ganglia were cut, except for the mesothoracic wing nerve 3A (meso-Nv3A), and the cercal nerves. See Jacob and Hedwig (2015) for details.

Exposed nervous tissue was rinsed with saline (in mmol l^{-1}: NaCl 140; KCl 10; $CaCl_2$ 7; $NaHCO_3$ 8; $MgCl_2$ 1; TES 5; D-trehalose dehydrate 4) adjusted to pH 7.4. To elicit fictive singing, glass capillaries filled with either eserine salicylate (10^{-2} mol l^{-1}) for *Gryllus*, or a mixture of eserine salicylate (10^{-2} mol l^{-1}) and nicotine (10^{-3} mol l^{-1}; Sigma-Aldrich, St Louis,

MO, USA) for *Teleogryllus*, in saline were inserted into the ventral protocerebrum and the solution was pressure injected (Pneumatic PicoPump PV820, WPI, Sarasota, FL, USA). See Wenzel and Hedwig (1999) and Schöneich and Hedwig (2012) for details. The efficacy of pharmacological stimulation in *Gryllus* species was 80%; in *Teleogryllus* 50% of males generated a mixture of all song types, and 24% of males generated a pure calling song (N=34).

The singing motor pattern was recorded from the meso-Nv3A, see Jacob and Hedwig, (2015) for details, which contains the axons of the front wing opener and closer motoneurons (Kutsch and Huber 1989; Poulet and Hedwig 2003). During singing the nerve recording reliable showed the rhythmically alternating spike activity of these two types of motoneurons. We identified the opener-motoneurons as the one that were always activated first and followed by the activity of the closer-motoneurons. We used a double-hook electrode made from 100 µm platinum wire and amplified the signal with a differential AC amplifier (Model 1700; A-M Systems, Sequim, WA, USA).

Intracellular recordings of the ascending opener interneuron in the A3 abdominal ganglion

The A3 ganglion was stabilized between a stainless-steel platform and a tungsten ring. Microcapillaries were pulled (DMZ-Universal Puller, Zeitz-Instruments, Martinsried, Germany) from thick-walled borosilicate glass tubes (ID 0.58 mm, OD 1.0 mm; Hilgenberg GmbH, Malsfeld, Germany). Intracellular recordings were made in bridge mode (SEC10-05LX amplifier; NPI, Tamm, Germany), sampled at 40 kHz per channel (Micro1401 mk II, CED, Cambridge, U.K.). A3-AO interneurons were recorded at the midline in the posterior region of the A3 ganglion at a depth of 25-40 µm and along the main neurite at a depth of 70-100 µm; measured with an Absolute Digimatic Depth Gauge (Mitutoyo UK, Coventry, U.K.) attached to the micromanipulator.

The neurons identified in this work were considered to belong to the singing-CPG according to criteria established by Marder and Calabrese (1996): 1) The neurons are active in time with the singing motor pattern; 2) The neurons initiate, terminate, or change the expression of the ongoing singing motor activity; 3) The neurons have direct or oligosynaptic connections with the relevant motoneurons.

Neuron morphology

Fluorescent dyes were iontophoretically injected into recorded neurons by constant hyperpolarizing current injection (0.5–5 nA, up to 20 min; for 0.5% Alexa 568 hydrazide sodium salt [Molecular Probes Inc., Eugene, OR, USA] or 1% Lucifer Yellow [Sigma-Aldrich, St Louis, MO, USA]) or by depolarizing pulses (2-3 nA, 200 ms duration, 3 Hz, up to 60 min; for 2-4% neurobiotin [Vector Laboratories, Burlingame, CA, USA]). Histological processing followed conventional protocols (Schöneich et al. 2011; Schöneich and Hedwig 2012). The whole-mount preparations were scanned with a confocal laser-scanning microscope (Leica SP5, Wetzlar, Germany). The morphology of neurons was reconstructed from the confocal image stacks using the Simple Neurite Tracer plugin in ImageJ (National Institutes of Health, Bethesda, MD, USA). All neurons presented here were stained with neurobiotin, unless otherwise stated. Since, the neurons are dye-coupled a short 10 min protocol of neurobiotin injection was performed. This was sufficient to stain the neuron up to T2 but not the dye-coupled neuron. The images obtained were compared with stainings obtained with Alexa 568 and Lucifer Yellow (data not shown), which are less reliable in showing dye-coupling between neurons when they are carried out for a few minutes. “Ipsilateral” and “contralateral” are used in relation to the neuron’s cell body. We will refer to the A3-AO homologues of the species as A3-$AO_{species}$, e.g. the A3-AO in *G. bimaculatus* will be labelled A3-AO_{bimac} and in *G. assimilis* A3-AO_{assim}.

Data analysis

Neurophysiological recordings were analyzed with CED Spike2 software (CED, Cambridge, UK) and with NEUROLAB (Knepper and Hedwig 1997). In case of song recordings for each male, three 10-minute time-windows with stable singing activity at the beginning, middle and end of one overnight singing period were chosen and the mean and standard deviation ($\bar{x}$±SD) of song parameters were calculated using the burst analysis feature of Spike 2 (Jacob and Hedwig 2016).

For analysis of A3-AO activity, the onsets of wing-opener and wing-closer motoneuron activity were used as temporal references. In the fictive singing motor pattern, the pulse period corresponds to the time between the first spike of two consecutive wing-closer bursts. The start of the ramp depolarization before singing episodes was established as the moment when the membrane potential differed by one SD from the mean resting amplitude for 10 ms subsequently. The duration of the ramp was measured from its start to the moment when the rising phase of the burst depolarization of the A3-AO started, the final amplitude of the ramp was also measured at this point. The rising phase was identified visually by the much faster membrane potential change of the neuron.

During the rhythmic membrane potential changes two features of the neuronal activity were measured. First, the time from the peak of the hyperpolarization to the moment of transition, named here hyperpolarization-to-transition time (H-to-T). Second, the time from the transition to the first spike of the burst depolarization, named here transition-to-spike (T-to-S). The transition moment was identified based on the speed of the rising membrane potential of the A3-AO, the arrowheads mark the transition point. Given the duration of the

T-to-S interval and the corresponding change in the depolarization, we calculated the rate of membrane potential change (mV/ms) at the start of a spike burst.

For the rebound depolarization after a hyperpolarization induced by current injection, the latency was measured between the end of the hyperpolarization current pulse and the occurrence of the 1^{st} spike of the rebound. The amplitude of the rebound was measured between the resting membrane potential and the peak of the depolarization.

Normally distributed data are given as $\bar{x}$±SD; when normality tests failed the median and interquartile range (IQR: 25^{th} percentile / 75^{th} percentile) is presented. In pooled data sets, each contributing animal is equally represented (N, number of animals; n, number of stimulations or events). For statistical analysis, we used GraphPad Prism 6 (GraphPad Software, Inc., La Jolla, CA, USA).

Results

Five cricket species were chosen due to their very distinctive calling song patterns, with pulses grouped in chirps or complex songs with chirps and trills (Figure 1). They were selected from the genus, *Teleogryllus* or *Gryllus*, with *Gryllus* species from the European or North American clade (Huang et al. 2000; Figure 1A), recordings of the calling songs are shown in Figure 1B.

In the calling songs of *G. bimaculatus* and *G. assimilis* sound pulses with a constant pulse rate are grouped in chirps, which are repeated regularly. For *G. rubens* trills are typical, i.e. long sequences of sound pulses with a constant pulse rate (Figure 1B). In *T. commodus* the calling song consists of two subsections, a chirp followed by one or four long trills. Also, in *T. oceanicus*, the song has two subsections; a trill is followed by a series of chirps. In both species the pulse rate differs between chirps and trills, and the two different subsections are arranged into a larger repeating unit of the song, called a phrase (Figure 1B), according to the

241 classification of song subsections by Bentley and Hoy (1972). A summary of the song
242 characteristics is presented in Table 1.

243 During fictive singing the pulse pattern is revealed in the rhythmic neuronal activity
244 of meso-Nv3A with alternating bursts of wing-opener and wing-closer motoneurons (Figure
245 1C).

246

247 *Comparative morphology of the ascending opener interneuron (A3-AO)*

248 The A3-AO neuron has a very similar structure in all the studied species (Figure 2). The
249 cell body is located ventrally in the posterior lateral margin of the A3 ganglion (Figure 2A,
250 arrow 1). The primary neurite ascends from the cell body to the neuropil 70-100 μm below
251 the dorsal surface; it runs towards the midline and crosses to the contralateral side (Figure
252 2A, arrow 2). At the midline an extensive dendritic branching pattern spreads from the
253 primary neurite anteriorly 25-40 μm beneath the surface (Figure 2A, arrow 3), and some finer
254 dendrites project posteriorly (Figure 2A, arrow 4). The axon arises from the primary neurite,
255 it bends laterally towards anterior and projects at the margin of the contralateral connective
256 towards the thoracic ganglia (Figure 2A, arrow 5). In the metathoracic ganglion complex
257 ($T3_{A1/A2}$), 4 to 7 prominent axon collaterals project dorsally towards the midline (Figure 2A,
258 arrow 6), in the mesothoracic ganglion (T2) a further 2 to 5 smaller collaterals project in a
259 similar manner (Figure 2A, arrow 7). The axon continues to the prothoracic ganglion (T1);
260 however, details of the structure could not be revealed. In all *Gryllus* species, the A3-AO
261 occurs as one bilateral pair of neurons, showing dye coupling.

262 Besides these similarities among the A3-AO neurons in *Gryllus,* there are also some
263 differences. $A3\text{-}AO_{bimac}$ (N=5; Figure 2A) has a very symmetrical dendritic branching pattern
264 in the anterior region of the A3 ganglion, however in the two North-American species
265 dendrites are more branched on the contralateral side. In the $T3_{A1/A2}$, the $A3\text{-}AO_{assim}$ has

fewer and finer dendrites, restricted to the midline of the ganglion (N=8; Figure 2A). In A3-AO_{rubens}, several axon collaterals in the $T3_{A1/A2}$ project towards the lateral region of the ganglion (N=8; Figure 2A). The extensive dendritic arborization in the A3 ganglion and axon collaterals in *Teleogryllus* are very similar to the A3-AO_{bimac}. As a fundamental difference to *Gryllus*, in *Teleogryllus* the number of A3-AO neurons is higher. In *T. commodus* a second pair of bilateral interneurons was always stained via dye coupling in recordings with neurobiotin (N=2) or Alexa 568 and LY (N=2). In three out of four *T. oceanicus* stainings of A3-AO_{ocean} with neurobiotin (N=2) or with Alexa 568 (N=1) three cell bodies (Figure 2C, left panel) were labelled, whereas in one animal two cell bodies were labelled on the same side (Figure 2C, right panel; Alexa 568).

Activity of A3-AO interneuron during fictive calling song

The stereotypical pattern of the motor activity allowed an identification of the corresponding song patterns (Figure 1C) and to quantify the features of the singing activity (Table 1). During fictive singing the pulse period across the species increased by 4-30%, however the characteristics and temporal organization of the fictive calling song corresponded to the natural calling song of each species (Table 1).

In the genus *Gryllus*, brain stimulation induces reliably calling song motor pattern. However, in the genus *Teleogryllus* that was not the case. In *T. commodus* (N=17), only 4 generated sustained period of calling song with 13 male generating mixed motor patterns, i.e. the production of long chirps, resembling the aggressive song or a mixture of calling and courtship songs (Loher and Rence 1978; Paripovic et al. 1996). In *T. oceanicus*, 4 out of 17 generated sustained periods of fictive calling song.

In all species, the A3-AO interneuron was identified by its rhythmic activity in phase with the wing-opener motor pattern (Figure 3). Prior to each singing episode (chirps or trills)

a gradual increase in membrane potential (ramp depolarization) occurred that culminated with the start of the burst depolarization of the A3-AO (Figure 3, Figure 4 highlighted in blue, and Table 2). During the intervals between singing episodes spiking ceased and there was only weak synaptic activity. A single opener-closer cycle is characterized by a rapid depolarization of A3-AO, preceding the wing-opener activity (Figure 3Aii-Eii, open circles), followed by a hyperpolarization, preceding the wing-closer activity (Figure 3Aii-Eii, closed circles). Recordings from the main neurite revealed a burst of spikes of 0.3-1.2 mV amplitude riding on top of a 10-18 mV amplitude depolarization (arrowheads in Figure 3Aii-Eii). In all species, the latency between the first spike of an A3-AO burst and the subsequent wing-opener activity is very short and stable (9-12 ms; Table 3). Besides these general features, the neurons exhibit species-specific characteristics, which are summarized in Figure 3, Figure 4, Table 2 and 3.

In *G. bimaculatus*, each chirp is initiated by a gradual ramp depolarisation, it starts 42±6.4 ms before a chirp and reaches an amplitude of 6±0.5 mV at the beginning of the pulse pattern (Figure 3Aii, 4Ai blue highlight; Table 2; N=5 animals, n=50 chirps). For each pulse period the membrane potential oscillations of A3-AO_{bimac} (Figure 3A, 4A) consist of a 17.5±2.1 mV amplitude depolarization generating a burst of 4-6 spikes followed by a 9.2±2.5 mV hyperpolarization (Table 3). The hyperpolarisation-to-transition (H-to-T) took 17±6.7 ms and the transition-to-spike (T-to-S) took 4.1±1.7 ms (N=5, n=50; Table 2), the rise of the membrane potential to the first spike of a burst occurred with 4.3 mV/ms.

In *G. assimilis*, the ramp depolarisation starts 40±7 ms before a chirp and reaches an amplitude of 4.3±1.3 mV (Figure 3Bii, 4Bi and Table 2; N=10, n=100). During a chirp the membrane potential is maintained at 2-4 mV above the resting potential while the activity of A3-AO_{assim} (Figure 3B) varies during the chirp pattern. A sequence of 5-8 pronounced depolarization-repolarization cycles is superimposed on the elevated membrane potential.

316 The depolarization amplitude of the first and last pulse is the smallest, 11±2 mV and 10.4±3.1
317 mV, respectively (Table 3; N=10 animals, n=100 chirps), while the middle pulses have a
318 mean amplitude of 14.9±4.6 mV (Figure 3B and Table 3: N=10, n=100). The last burst is
319 terminated by a pronounced transient hyperpolarization of 11.7±3.1 mV preceding the final
320 closer activity (N=10, n=100; Table 3). As the second burst has the most pronounced
321 depolarisation its transition phase was analysed in detail. For this burst the H-to-T took
322 9.1±0.6 ms, the T-to-S was 1.9±0.5 ms (N=10, n=100; Table 2), and the rise of the membrane
323 potential to the first spike of this burst occurred with 7.6 mV/ms.

324 In *G. rubens*, the ramp depolarisation begins 21±2.1 ms before a trill and reaches
325 2.9±0.4 mV (Figure 4Ci and Table 2; N=10, n=70). During a trill, the A3-AO_{rubens} membrane
326 potential rhythmically oscillates in phase with the pulse pattern (Figure 3C). Preceding each
327 subsequent opener activity, the neuron generates a 10.5±4.7 mV amplitude depolarization
328 with 2-4 spikes (Table 3; N=10, n=70 trills). Each depolarization is followed by a
329 hyperpolarization of 8.1±3.5 mV (Table 3; N=10, n=70) preceding the following closer
330 activity. H-to-T takes12±3.3 ms and T-to-S takes 4.7±2.3 ms (N=10, n=70; Table 2); at the
331 start of a burst the membrane potential changes at a rate of 2.3 mV/ms.

332 In *T. commodus* (Figure 3D) the rhythmic activity of A3-AO_{comm} mirrors the chirp
333 and trill sections. The ramp depolarisation starts 101±11 ms before a chirp and reaches an
334 amplitude of 4.1±2.2 mV (Figure 4Di and Table 2; N=4, n=40). During chirps each
335 depolarization of 16.4±4.1 mV (Table 3; N=4, n=40 song phrases) generates 3-7 spikes
336 followed by a hyperpolarization of 10.1±3.2 mV (Table 3: N=4, n=40). During trills, the
337 amplitude of the depolarization is 13.4±3.8 mV (Table 3; N=4, n=40), with 3-9 spikes,
338 followed by a 6.5±2.5 mV hyperpolarization (Table 3; N=4, n=40). The H-to-T interval is
339 35±4 ms during a chirp and 14±2.1 ms during a trill, the T-to-S interval is 7.5±0.5 ms during
340 a chirp and 4.5±1.2 ms during a trill (N=4, n=40; Table 2). The membrane potential at the

beginning of a burst increases with 2.2 mV/ms during a chirp and with 3 mV/ms during a trill; N=4, n=40).

In *T. oceanicus*, (Figure 3E) the rhythmic activity of A3-AO_{ocean} clearly reveals the trill and the chirp sections of the song (Figure 3E). The ramp depolarisation begins 51±15 ms before a trill reaching an amplitude of 2.8±0.1 mV (Figure 4Ei and Table 2; N=4, n=40). During the trill the rhythmic depolarization preceding the opener activity is 15.9±5.2 mV in amplitude (Table 3; N=4, n=40 song phrases) generating 4-6 spikes, each depolarization is followed by a hyperpolarization of 9.2±3.9 mV (Table 3; N=4, n=40). During the chirps the depolarization has an amplitude of 13.6±4.2 mV (Table 3; N=4, n=40) generating 2-5 spikes, followed by a hyperpolarization of 7.2±3.3 mV (Table 3; N=4, n=40). H-to-T interval is 35±4 ms during the trill section and 18±0.1 ms in the chirp section. The T-to-S interval is 4.2±0.4 ms in the trill section and 3.8±0.2 ms in the chirp section (N=4, n=40; Table 2). At the beginning of a burst the membrane potential increases with 3.7 mV/ms in the trills and with 3.6 mV/ms during the chirps.

Initiation and modulation of singing motor patterns by intracellular A3-AO stimulation

In all species, injection of depolarizing current (4 nA, 155 ms) into the main neurite of the A3-AO interneuron elicited oscillations of the membrane potential (Figure 5A-E) accompanied by alternating opener–closer motoneuron activity in the meso-Nv3A. Motor activity ceased with the end of the current injection.

We analyzed the pulse periods and compared the motor activity of the fictive song pattern (blue) with the activity induced by A3-AO current injection (orange), taking the wing-closer activity as reference (see *inset* Figure 5Aiii). In *Gryllus* species, the pulse periods of fictive singing as elicited by pharmacological brain stimulation (see Methods) were not significantly different from the pulse periods elicited by A3-AO stimulation. In *G.*

bimaculatus, the median pulse period during fictive singing was 42 ms (IQR: 39.2 ms/44.8 ms, N=4), and for A3-AO stimulation 39.9 ms (IQR: 36.4 ms/45.5 ms; Kolmogorov-Smirnov test for equality of distribution functions: p=0.485, N=4, n=5 stimuli/animal, Figure 5Aiii). In *G. assimilis*, the median pulse period during fictive singing was 20.3 ms (IQR: 16.1 ms/23.8 ms; N=4) and during A3-AO stimulation 20.3 ms (IQR: 16.8 ms/23.8 ms; Kolmogorov-Smirnov test: p=0.541, N=4, n=5 stimuli/animal, Figure 5Biii). For *G. rubens*, the median pulse period of fictive singing was 26 ms (IQR: 25 ms/27 ms; N=4) and for A3-AO current injection 24 ms (IQR: 21 ms/26 ms; Kolmogorov-Smirnov test: p=0.159, N=4, n=10 stimuli/animal, Figure 5Ciii).

In *Teleogryllus* species the fictive calling song elicited by brain stimulation had a bimodal distribution of pulse periods due to the generation of chirps and trills (Figure 5Di-Ei). In both species, the first peak of the distribution corresponds to the song phrase, with the highest pulse rate (*T. commodus*: median 41.8 ms [IQR: 37.4 ms/46.2]; *T. oceanicus*: median 47.3 ms [IQR: 40.7 ms/50.6 ms]; Figure 5Diii-Eiii, orange; N=4). The second peak of the distribution corresponds to the song phrase with the lowest pulse rate (*T. commodus*: median 72.6 ms [IQR: 66 ms/79.2 ms]; *T. oceanicus* median 70.4 ms [IQR: 66 ms/ 77 ms]; Figure 5Diii-Eiii, blue; N=4). Intracellular A3-AO stimulation induced shorter pulse periods than either of these: the median pulse period was 28.6 ms (IQR: 25.3ms/30.8 ms) in *T. commodus* and 34.1 ms (IQR: 28.6 ms/42.9 ms) in *T. oceanicus*. The pulse periods correspond most closely to the faster sections of the fictive song but they were significantly shorter (Kolmogorov-Smirnov test: *T. commodus* p=0.002, N=4, n=10 stimuli/animal, Figure 5Diii; *T. oceanicus* p=0.032, N=4, n=10 current stimulations per animal, Figure 5Eiii).

In the fictive motor pattern, slower song sections, in terms of pulse period, always precede the faster sections. We subsequently tested the response of A3-AO to 3.4 s current pulses of +3 nA, to determine if both the slow and fast sections of the songs could be elicited.

In both *Teleogryllus* species, sustained injection of depolarizing current in A3-AO induced different pulse periods.

In *T. commodus* (Figure 6Ai), three different types of membrane potential oscillations occurred during long A3-AO depolarisation. The motor pattern started with a fast section composed of 3-6 pulses (Figure 6Aii, see figure legend for details on median pulse period), followed by a slow section with 5-10 pulses (Figure 6Aii), and a subsequent continuous fast section (Figure 6Aii). The fast sections had a pulse period similar to a trill section and the slow sections had pulse periods similar to a chirp section.

Three different types of membrane potential oscillations representing the pulse pattern also occurred in *T. oceanicus* (Figure 6Bi) following intracellular A3-AO stimulation. As compared to fictive singing, activity started with an unusually fast rhythm (Figure 6Bii, see figure legend for details on median pulse period), followed by a slower section (Figure 6Bii) and finally by section with an intermediate rhythm (Figure 6Bii). The intermediate section had a pulse period similar to a chirp section and the slow sections had pulse periods similar to a trill section. The fast section elicited by the current injection is surprising in the context of the calling song of *T. oceanicus*.

Besides this the organization of the resulting song pattern was different from the fictive calling song since the silent intervals between the trills and chirps were lacking (Figure 6).

Current injection in A3-AO imposes artificial song patterns

Spike activity of A3-AO is sufficient to determine the temporal structure of song episodes in all five species, as demonstrated by intracellular injection of +4 nA current of different duration and rates (Figure 7). In species with short chirps like *G. bimaculatus* and *G. assimilis*, depolarization for 1.6 s caused the membrane potential of A3-AO_{bimac} and A3-

AO_{assim} to oscillate continuously in the species-specific pulse pattern accompanied by singing motor activity. Fictive singing activity, however, was not organized in chirps; its duration rather was determined by the current injection pattern (Figure 7Ai-Bi). In the species with long calling songs, *G. rubens* and both *Teleogryllus* species, short current pulses (170 ms in *G. rubens* and *T. oceanicus* and 300 ms in *T. commodus*) elicited A3-AO membrane potential oscillations during the current injection, accompanied by short bouts of singing motor activity that normally would not occur (Figure 7Ci-Ei).

In all species tested the duration of singing episodes was controlled by activation of the A3-AO, the intracellular current pulses set the temporal structure of the singing pattern. Furthermore, in *Teleogryllus*, the fast and slow sections of the song were induced by long current injection. These data suggest that the normal organization of chirps and trills is not determined just by the A3-AO activity but by additional neurons within the network which control and drive the A3-AO interneuron.

Reset of chirp pattern

In *Gryllus* species, depolarizing A3-AO with current pulses (4nA, 100 ms and 500 ms duration) during fictive singing modified the ongoing song pattern (Figure 8). In *G. bimaculatus* and *G. assimilis* the stimulation reset the ongoing chirp rhythm (Figure 8A-B). Injection of 100 ms (*G. bimaculatus*: N=5, n=88; *G. assimilis*: N=6, n=97) and 500 ms (*G. bimaculatus*: N=3, n=30; *G. assimilis*: N=6, n=53) pulses at different moments of the chirp cycle revealed a linear relationship between the stimulation phase within the chirp cycle and the shift of the chirp rhythm (Figure 8Aii-Bii). In *G. rubens* there was a linear relationship between the stimulation phase and the shift of the trill rhythm for 500 ms current pulses ($y=2.375x+0.042$, $r^2=0.18$, N=5, n=62 trills) but not for the 100 ms pulses ($y=0.749x+0.203$, $r^2=0.11$, N=6, n=86 trills; Figure 8Ci,ii). In both cases r^2 was low, which could be due to the

441 intrinsic variability in the fictive trill pattern in this species. In *Teleogryllus* species, current
442 injection altered the ongoing singing activity (not shown), however the variability of the
443 fictive calling song pattern did not allow us to calculate a reliable phase-response curve.

444 *Response of A3-AO to hyperpolarizing current pulses*

445 In *G. bimaculatus*, hyperpolarizing current injection in the main dendrite of A3-AO
446 demonstrated a post-inhibitory rebound that subsequently initiated the generation of singing
447 motor activity (Schöneich and Hedwig 2012). We analyzed to what degree the A3-AO
448 interneuron of the species shared this property.

449 In all five species injections of -5 nA pulses for 1s in the main dendrite were followed
450 by cycles of depolarization and hyperpolarization accompanied by wing-opener and wing-
451 closer motor neuron activity. The rebound depolarization as measured from the resting
452 membrane potential to the peak of the rebound had an amplitude of 3-10 mV (Figure 9,
453 vertical arrows) and elicited 1-3 spikes. The subsequent hyperpolarization had an amplitude
454 of 0.5-3 mV (Figure 9Ai-Ei). However, the shape and amplitude of the elicited
455 depolarization-hyperpolarization cycles were smaller in comparison to the membrane
456 potential oscillations during fictive singing.

457 We measured the latency of the first spike generated after release from
458 hyperpolarization by -0.5 nA to -10 nA (Figure 9Aii-Eii, horizontal arrows) and calculated
459 the linear regression functions for the data. In all *Gryllus* species, the regression functions
460 indicate a tendency for larger amplitude negative currents inducing longer rebound latencies
461 (Figure 9Aii-Cii) in *Teleogryllus* data were more variable and a clear tendency cannot be
462 reported (Figure 9 Dii, Eii).

463

464 **Discussion**

We analyzed the structure and function of the A3-AO neurons in five cricket species that generate different calling songs to reveal if and how species-specific behavior is reflected at the level of an identified CPG-interneuron.

The study of neuronal homology across closely-related species requires combining different levels of evidence (Weiss and Kupfermann 1976; Arbas et al. 1991; Katz 2007, 2015, 2016; Niven and Chittka 2016; Katz and Hale 2017). Here, we use comprehensive behavioral, neurophysiological and structural data to reveal the homology of the A3-AO neuron in crickets. Our results suggest that in all five species, the interneuron can be considered to belong to the singing-CPG according to the criteria for identifying CPG components set out by Marder and Calabrese (1996).

Neurophysiological evidence for homology of function

The A3-AO interneuron showed similar neurophysiological characteristics across the five species and at least four shared features can be surmised:

1) A ramp depolarization of the membrane potential occurs before the start of chirps or trills. A gradual ramp depolarization of the A3-AO preceded the generation of a chirp or trill. This depolarization could be imparted by the descending command neurons, driving the singing-CPG with tonic spike activity (Hedwig 2000), similarly to the swimming-CPG in *Tritonia* (Frost and Katz 1996). Alternatively, the ramp depolarization may be controlled by neurons of the singing network, housed in the posterior ganglia (Jacob and Hedwig 2016), which control the chirp pattern of the songs.

2) Activity is tightly coupled to the calling song pattern. Depolarization and spike activity precede the wing-opener motoneuron activity followed by a repolarization/hyperpolarization preceding the wing-closer motoneurons. The depolarization and spike burst of A3-AO is always in phase with the wing-opener activity and the

hyperpolarization to the wing-closer activity. Additionally, the neurons show species-specific characteristics, in terms of the shape of the membrane potential oscillations, the steepness and amplitude of the start of the bursts and the number of action potentials per depolarization. These differences might be crucial for the timing of the species-specific pulse patterns since the activity of the A3-AO seems to inhibit the closer-interneurons during the opener-phase. This subsequently triggers the closer-interneuron activity (Schöneich and Hedwig 2012), which drives the closer-motoneurons to produce a sound pulse.

At the current level of analysis, it is impossible to reveal to what degree the species-specific characteristics of membrane potential changes are due to intrinsic properties of the A3-AO or due to synaptic inputs driving the neuron. We expect that a combination of specific adaptations of A3-AO conductances and network properties will contribute to the species-specific patterns (Selverston 1980).

3) A3-AO is an element of the singing CPG. Its activity elicits the species-specific pulse-pattern of the calling song; in Gryllus it resets the timing of the chirps/trills. Activation of the interneuron by current injection was sufficient to initiate and maintain rhythmic activity of the wing motoneurons typical of the species-specific singing motor pattern and to reset the chirp pattern in the *Gryllus* species. In *Teleogryllus*, three significantly different pulse periods occurred upon long current injections. In *T. commodus*, the structure of the induced motor pattern had a trill-chirp-trill organization and resembled the courtship song (Loher and Rence 1978; Paripovic et al. 1996).

Moreover, stimulation of the neuron with sequences of current injections imposed an artificial song structure in all species. The A3-AO interneuron could be a network element that determines the temporal structure of species-specific song patterns. However, while the timing of song episodes is determined by A3-AO activation, the neuron depends on other synaptic inputs from the singing network to organize the chirp/trill pattern and stabilize the

normal song pattern. This is in accordance with the finding, that the A3 ganglion in *G. bimaculatus* houses part of the pulse-timer network for singing, whereas the temporal pattern of the chirps is controlled by the posterior ganglia (Jacob and Hedwig 2016).

4) The neuron generates a rebound depolarization after inhibition. The function of the singing-CPG is thought to be based on a reciprocal inhibitory network (Bentley 1969; Schöneich and Hedwig 2012). The ion channels involved in driving the rebound are not yet identified. Our data shows, there is a tendency for the latency of the first spike of the rebound depolarization to become longer with the amplitude of the hyperpolarizing current in the Gryllus species; the effect is quite variable and appears to plateau at -8 nA. Precluding any final conclusion, this might point to the presence of the transient potassium current I_A (Hartline and Gassie 1979; Harris-Warrick et al. 1995a, 1995b; Pirtle and Satterlie 2004). These currents are known to be involved in the modulation of the timing of activity of neurons in several motor networks (Tierney and Harris-Warrick 1992; Harris-Warrick et al. 1995a; Ping et al. 2011). The ion channels involved in driving the rebound will need to be analyzed using voltage-clamp and pharmacological experiments.

Structural evidence for homology and functional implications

Homology based on conserved neuron morphology across species is common and accepted in invertebrate motor (Wilson et al. 1982; Arbas 1983a, 1983b; Schütze and Elsner 2001) and sensory systems, for example the Omega-neuron 1 in the auditory pathway of crickets (Casaday and Hoy 1977; Römer et al. 1988; Stumpner and von Helversen 2001; Farris et al. 2004). The shared structural features of the A3-AO neuron support homology as the most parsimonious explanation: 1) the conserved position of the cell body, located on the posterior ventral side of the A3 ganglion. 2) The location and shape of the extensive anterior dendritic branches and the small posterior dendrites dorsally in A3. 3) The axon projection

through the most lateral part of the contralateral connective towards the prothoracic ganglion. 4) Axon collaterals present in ganglion T3 and T2. 5) Dye coupling that reliably occurs between the left-right neurons.

A comparison of the A3-AO structure indicates that its “gestalt” is the same across species, which must be embedded in the species-specific organization of the singing network. The neurons are likely subject to a conserved developmental program, determining the position of the cell body and the shape of the dendritic and axonal ramifications. Specific differences in this program may facilitate the evolution of song patterns. A final proof for homology would require tracing the A3-AO to the same ganglion mother cell (Bate et al. 1981; Pearson et al. 1985).

In *Gryllus* species dye coupling revealed that A3-AO neurons are present as one pair of bilateral neurons (Schöneich and Hedwig 2011, 2012). Also, our data support the presence of a single pair of bilateral A3-AO neurons, however due to the nature of the experiments, the presence of a second pair of the A3-AO neuron cannot be excluded. In *Teleogryllus* dye coupling demonstrated the existence of at least 2 pairs of A3-AO neurons, we hypothesise that this might be related to the different song rhythms in *Teleogryllus* species, pointing to a difference between the clades of *Gryllus* and *Teleogryllus* (Huang et al. 2000; Desutter-Grandcolas and Robillard 2001). The larger number of neurons involved in pattern generation might be a way of increasing the synaptic strength to drive postsynaptic neurons, or increasing the reliability of song pattern generation, or allowing more flexibility for the generation of trills and chirps and point to different evolutionary ways to adjust network properties.

Species-specific differences in the dendritic branching pattern may reflect the strength of synaptic connectivity (Macagno et al. 1973; Goodman 1978; Arbas et al. 1991). Within the singing network there is clear evidence for species-specific differences in the distribution,

size and density of dendrites and axon collaterals within the neuropil of the A3 and thoracic ganglia, respectively.

Axon collaterals and activity of the A3-AO interneuron

Across all species the A3-AO neuron showed characteristic projections of its axon collaterals towards the midline of the $T3_{A1/A2}$ ganglion, which may overlap with descending interneurons of the singing network (Hennig 1989, 1990; Schöneich and Hedwig 2012). The arrangement and density of the main axonal collaterals in the $T3_{A1/A2}$ have characteristic species-specific differences, in contrast to the more similar axonal branching pattern in A3 and in T2. The A3-AO axon gives off small collaterals in the dorsal neuropil of the T2 ganglion, which are remarkably similar in the different species. These collaterals could overlap with the dorsal dendrites of the wing-opener motoneurons (Ewing and Hoyle 1965; Bentley and Kutsch 1966; Hennig 1989; Kutsch and Huber 1989), and A3-AO could be a "premotor" interneuron (Robertson and Pearson 1983, 1985; Robertson 1987). Although evidence for synaptic connections has not yet been obtained, in all species the latency of the A3-AO spike and the wing-opener motoneuron activity, as recorded in meso-Nv3A, was short and stable. This might be an indicator for a direct link between the A3-AO interneuron and the motoneurons. As at this stage of processing the pulse pattern is already determined, an A3-AO to motoneuron connection could be a highly conserved part of the singing network with little species-specific adaptations.

Conclusions for species-specific adaptations underlying singing

In an evolutionary neurobiological approach, significant species-specific differences between CPG-networks need to be revealed to understand the evolutionary mechanisms leading to novel motor patterns. As the fundamental characteristics of the A3-AO are

590 conserved, our data indicates that the fine-tuning of cellular and network properties are key to
591 understand how species-specific song patterns emerged. This imposes a fundamental problem
592 of such a network analysis, which will require the combination of neurophysiological and
593 neurogenetic tools to be achieved.
594

595 **References**

596 **Alexander R**. Evolutionary change in cricket acoustical communication *Evolution* 16: 443–
597 467, 1962.

598 **Arbas EA**. Thoracic morphology of a flightless Mexican grasshopper, *Barytettix psolus*:
599 Comparison with the locust, *Schistocerca gregaria*. *J Morphol* 176: 141–153, 1983a.

600 **Arbas EA**. Neural correlates of flight loss in a mexican grasshopper, *Barytettix psolus*. II.
601 DCMD and TCG interneurons. *J Comp Neurol* 216: 381–389, 1983b.

602 **Arbas EA**, **Meinertzhagen IA**, **Shaw SR**. Evolution in nervous systems. *Annu Rev Neurosci*
603 14: 9–38, 1991.

604 **ASAB Ethics Committee**. Guidelines for the treatment of animals in behavioural research
605 and teaching. *Anim Behav* 53: 229–234, 1997.

606 **Bate M**, **Goodman CS**, **Spitzer NC**. Embryonic development of identified neurons: segment
607 specific differences in the H cell homologues. *J Neurosci* 1: 103–106, 1981.

608 **Bentley DR**. Intracellular activity in cricket neurons during generation of song patterns. *Z vgl*
609 *Physiol* 283: 267–283, 1969.

610 **Bentley DR**, **Hoy RR**. Genetic control of the neuronal network generating cricket
611 (*Teleogryllus, Gryllus*) song patterns. *Anim Behav* 20: 478–92, 1972.

612 **Bentley DR**, **Kutsch W**. The neuromuscular mechanism of stridulation in crickets
613 (Orthoptera: Gryllidae). *J Exp Biol* 45: 151–64, 1966.

614 **Blankers T**, **Block R**, **Hennig RM**. Codivergence but Limited Covariance of Wing Shape
615 and Calling Song Structure in Field Crickets (Gryllus). *Evol Biol* 45: 144–55, 2017.

616 **Boughman JW**. How sensory drive can promote speciation. *Trends Ecol Evol*. 17(12): 571–
617 7, 2002.

618 **Capranica RR**. The untuning of the tuning curve: is it time? *Semin Neurosci* 4: 401–408,
619 1992.

620 **Casaday GB**, **Hoy RR**. Auditory interneurons in the cricket *Teleogryllus oceanicus*:
621 Physiological and anatomical properties. *J Comp Physiol A* 121: 1–13, 1977.
622 **Chagnaud BP**, **Baker R**, **Bass AH**. Vocalization frequency and duration are coded in
623 separate hindbrain nuclei. *Nat Commun* 2: 346, 2011.
624 **Clyne JD**, **Miesenböck G**. Sex-specific control and tuning of the pattern generator for
625 courtship song in *Drosophila*. *Cell* 133: 354–63, 2008.
626 **Crews D**. Species diversity and the evolution of behavioral controlling mechanisms. *Ann*
627 *Acad Sci* 807: 1–21, 1997.
628 **Desutter-Grandcolas L**, **Robillard T**. Phylogeny and the evolution of calling songs in
629 Gryllus (Insecta, Orthoptera, Gryllidae). *Zool Scr* 32: 173–183, 2001.
630 **Ding Y**, **Berrocal A**, **Morita T**, **Longden KD**, **Stern DL**. Natural courtship song variation
631 caused by an intronic retroelement in an ion channel gene. *Nature* 536: 329–332, 2016.
632 **Elsner N**, **Wasser G**. The Transition from Leg to Wing Stridulation in Two Geographically
633 Distinct Populations of the Grasshopper *Stenobothrus rubicundus*. *Naturwissenschaften* 82:
634 384–386, 1995.
635 **Endler JA**, **Basolo AL**. Sensory ecology, receiver biases and sexual selection. *Trends Ecol*
636 *Evol* 13: 415–420, 1998.
637 **Ewing A**, **Hoyle G**. Neuronal mechanisms underlying control of sound production in a
638 cricket: *Acheta domesticus*. *J Exp Biol* 43: 139–53, 1965.
639 **Farris HE**, **Mason AC**, **Hoy RR**. Identified auditory neurons in the cricket *Gryllus rubens*:
640 Temporal processing in calling song sensitive units. *Hear Res* 193: 121–133, 2004.
641 **Frost WN**, **Katz PS**. Single neuron control over a complex motor program. *Proc Natl Acad*
642 *Sci* 93: 422–426, 1996.
643 **Goodman CS**. Isogenic grasshoppers: Genetic variability in the morphology of identified
644 neurons. *J Comp Neurol* 182: 681–705, 1978.

Harris-Warrick RM, **Coniglio LM**, **Barazangi N**, **Guckenheimer J**, **Gueron S**. Dopamine modulation of transient potassium current evokes phase shifts in a central pattern generator network. *J Neurosci* 15: 342–358, 1995a.

Harris-Warrick RM, **Coniglio LM**, **Levini RM**, **Gueron S**, **Guckenheimer J**. Dopamine modulation of two subthreshold currents produces phase shifts in activity of an identified motoneuron. *J Neurophysiol* 74: 1404–20, 1995b.

Hartline DK, **Gassie D V**. Pattern generation in the lobster (*Panulirus*) stomatogastric ganglion: I. Pyloric Neuron Kinetics and Synaptic Interactions. *Biol Cybern* 33: 209–222, 1979.

Hedwig B. Control of cricket stridulation by a command neuron: efficacy depends on the behavioral state. *J Neurophysiol* 83: 712–722, 2000.

Hennig RM. Neuromuscular activity during stridulation in the cricket *Teleogryllus commodus*. *J Comp Physiol A* 165: 837–846, 1989.

Hennig RM. Neuronal control of the forewings in two different behaviours: Stridulation and flight in the cricket, *Teleogryllus commodus*. *J Comp Physiol A* 167: 617–627, 1990.

ter Hofstede HM, **Schöneich S**, **Robillard T**, **Hedwig B**. Evolution of a Communication System by Sensory Exploitation of Startle Behavior. *Curr Biol* 25: 3245–3252, 2015.

Hoikkala A, **Hoy RR**, **Kaneshiro KY**. High-frequency clicks of Hawaiian picture-winged *Drosophila* species. *Anim Behav* 37, Part 6: 927–934, 1989.

Hoikkala A, **Kaneshiro KY**, **Hoy RR**. Courtship songs of the picture-winged *Drosophila planitibia* subgroup species. *Anim Behav* 47: 1363–1374, 1994.

Hoy RR, **Hoikkala A**, **Kaneshiro K**. Hawaiian courtship songs: evolutionary innovation in communication signals of *Drosophila*. *Science* 240: 217–9, 1988.

Huang Y, **Ortí G**, **Sutherlin M**, **Duhachek A**, **Zera A**. Phylogenetic relationships of North American field crickets inferred from mitochondrial DNA data. *Mol Phylogenet Evol* 17: 48–

57, 2000.

Jacob PF, **Hedwig B**. Impact of cercal air currents on singing motor pattern generation in the cricket (*Gryllus bimaculatus* DeGeer). *J Neurophysiol* 114: 2649–60, 2015.

Jacob PF, **Hedwig B**. Acoustic signalling for mate attraction in crickets: Abdominal ganglia control the timing of the calling song pattern. *Behav Brain Res* 309: 51–66, 2016.

Kaneshiro KY. Sexual isolation, speciation and the direction of evolution. *Evolution (N Y)* 34: 437–444, 1980.

Katz PS. Evolution and development of neural circuits in invertebrates. *Curr Opin Neurobiol* 17: 59–64, ü2007.

Katz PS. Evolution of central pattern generators and rhythmic behaviours. *Phil Trans R Soc London B Biol Sci* 371: 1-12, 2016.

Katz PS. Phylogenetic plasticity in the evolution of molluscan neural circuits. *Curr Opin Neurobiol* 41: 8–16, 2016.

Katz PS, **Hale ME**. Evolution of Motor Systems. In: *Neurobiology of Motor Control: Fundamental Concepts and New Directions*, edited by Hooper SL, Büschges A. John Wiley & Sons, 2017.

Katz PS, **Harris-Warrick RM**. The evolution of neuronal circuits underlying species-specific behavior. *Curr Opin Neurobiol* 9: 628–33, 1999.

Knepper M, **Hedwig B**. NEUROLAB, a PC-program for the processing of neurobiological data. *Comput Methods Programs Biomed* 52: 75–77, 1997.

Kutsch W, **Huber F**. Neural basis of song production. In: *Cricket Behavior and Neurobiology*, edited by Huber F, Moore T, Loher W. New York: Cornell University Press, 1989, pp. 262–309.

Loher W, **Rence B**. The mating behavior of *Teleogryllus commodus* (Walker) and its central and peripheral control. *Z Tierpsychol* 46: 225–259, 1978.

Macagno ER, **Lopresti V**, **Levinthal C**. Structure and development of neuronal connections in isogenic organisms: variations and similarities in the optic system of *Daphnia magna*. *Proc Natl Acad Sci* 70: 57–61, 1973.

Marder E, **Calabrese RL**. Principles of rhythmic motor pattern generation. *Physiol Rev* 76: 687–717, 1996.

Mendelson TC, **Shaw KL**. Genetic and behavioral components of the cryptic species boundary between *Laupala cerasina* and *L. kohalensis* (Orthoptera: Gryllidae). In: *Genetics of Mate Choice: From Sexual Selection to Sexual Isolation*, edited by Etges WJ, Noor MAF. Springer Netherlands, pp. 301–310.

Mendelson TC, **Shaw KL**. Sexual behaviour: Rapid speciation in an arthropod. *Nature* 433: 375–376, 2005.

Montealegre-Z F, **Jonsson T**, **Robert D**. Sound radiation and wing mechanics in stridulating field crickets (Orthoptera: Gryllidae). *J Exp Biol* 214: 2105–17, 2011.

Muller HJ. Reversibility in evolution considered from the standpoint of genetics. *Biol Rev* 14: 261–280, 1939.

Niven JE, **Chittka L**. Evolving understanding of nervous system evolution. *Curr Biol* 26: R937–R941, 2016.

Otte D. Evolution of Cricket Songs. *J Orthoptera Res*: 25–49, 1992.

Paripovic I, **Hennig RM**, **Otto D**. Abdominal ventilatory pattern in crickets depends on the stridulatory motor pattern. *Physiol Entomol* 21: 223–230, 1996.

Pearson KG, **Boyan GS**, **Bastiani M**, **Goodman CS**. Heterogeneous properties of segmentally homologous interneurones in the ventral cord of locusts. *J Comp Neurol* 233: 133–145, 1985.

von Philipsborn AC, **Jörchel S**, **Tirian L**, **Demir E**, **Morita T**, **Stern DL**, **Dickson BJ**. Cellular and behavioral functions of fruitless isoforms in Drosophila courtship. *Curr Biol* 24:

242–251, 2014.

von Philipsborn AC, **Liu T**, **Yu JY**, **Masser C**, **Bidaye SS**, **Dickson BJ**. Neuronal control of *Drosophila* courtship song. *Neuron* 69: 509–22, 2011.

Ping Y, **Waro G**, **Licursi A**, **Smith S**, **Vo-Ba D-A**, **Tsunoda S**. *Shal/Kv4* channels are required for maintaining excitability during repetitive firing and normal locomotion in *Drosophila*. *PLoS One* 6: e16043, 2011.

Pirtle TJ, **Satterlie RA**. Cellular Mechanisms Underlying Swim Acceleration in the Pteropod Mollusc *Clione limacina*. *Integr Comp Biol* 44: 37–46, 2004.

Poulet JFA, **Hedwig B**. A corollary discharge mechanism modulates central auditory processing in singing crickets. *J Neurophysiol* 89: 1528–40, 2003.

Ritchie MG. Sexual Selection and Speciation. *Annu Rev Ecol Evol Syst* 38: 79–102, 2007.

Robertson RM. Interneurons in the flight system of the cricket *Teleogryllus oceanicus*. *J Comp Physiol A* 160: 431–445, 1987.

Robertson RM, **Pearson KG**. Interneurons in the flight system of the locust: Distribution, connections, and resetting properties. *J Comp Neurol* 215: 33–50, 1983.

Robertson RM, **Pearson KG**. Neural circuits in the flight system of the locust. *J Neurophysiol* 53: 110–28, 1985.

Römer H, **Marquart V**, **Hardt M**. Organization of a sensory neuropile in the auditory pathway of two groups of Orthoptera. *J Comp Neurol* 275: 201–215, 1988.

Schöneich S, **Hedwig B**. Neural basis of singing in crickets: central pattern generation in abdominal ganglia. *Naturwissenschaften* 98: 1069–73, 2011.

Schöneich S, **Hedwig B**. Cellular basis for singing motor pattern generation in the field cricket (*Gryllus bimaculatus* DeGeer). *Brain Behav* 2: 707–25, 2012.

Schöneich S, **Schildberger K**, **Stevenson PA**. Neuronal organization of a fast-mediating cephalothoracic pathway for antennal-tactile information in the cricket (*Gryllus bimaculatus*

745 DeGeer). *J Comp Neurol* 519: 1677–90, 2011.

746 **Schütze H**, **Elsner N**. Stridulatory pattern generation in acridid grasshoppers: metathoracic
747 interneurons in *Stenobothrus rubicundus* (Germar 1817). *J Comp Physiol A* 187: 529–540,
748 2001.

749 **Selverston AI**. Are central pattern generators understandable? *Behav Brain Sci* 3: 535-571,
750 1980.

751 **Shaw KL**. Polygenic inheritance of a behavioral phenotype: interspecific genetics of song in
752 the Hawaiian cricket genus *Laupala*. *Evolution* 50: 256–266, 1996.

753 **Shirangi TR**, **Stern DL**, **Truman JW**. Motor control of *Drosophila* courtship song. *Cell*
754 *Rep* 5: 678–686, 2013.

755 **Shirangi TR**, **Stern DL**, **Truman JW**. Motor Control of *Drosophila* Courtship Song. *Cell*
756 *Rep* 5: 678–686, 2016.

757 **Stumpner A**, **von Helversen D**. Evolution and function of auditory systems in insects.
758 *Naturwissenschaften* 88: 159–170, 2001.

759 **Tierney AJ**, **Harris-Warrick RM**. Physiological role of the transient potassium current in
760 the pyloric circuit of the lobster stomatogastric ganglion. *J Neurophysiol* 67: 599–609, 1992.

761 **Vedenina V**, **Fähsing S**, **Sradnick J**, **Klöpfel A**, **Elsner N**. A narrow hybrid zone between
762 the grasshoppers *Stenobothrus clavatus* and *Stenobothrus rubicundus* (Orthoptera:
763 Gomphocerinae): female preferences for courtship songs. *Biol J Linn Soc* 107: 383–397,
764 2012.

765 **Weiss KR**, **Kupfermann I**. Homology of the giant serotonergic neurons (metacerebral cells)
766 in *Aplysia* and pulmonate molluscs. *Brain Res* 117: 33–49, 1976.

767 **Wenzel B**, **Hedwig B**. Neurochemical control of cricket stridulation revealed by
768 pharmacological microinjections into the brain. *J Exp Biol* 202: 2203–2216, 1999.

769 **Wilson JA**, **Phillips CE**, **Adams ME**, **Huber F**. Structural comparison of a homologous

770 neuron in Gryllid and Acridid insects. *J Neurobiol* 13: 459–467, 1982.

771

Figure legends

Figure 1. Phylogenetic relationship of cricket species studied and their natural and fictive calling song patterns.

Simplified cricket phylogenetic tree derived from Huang et al. (2000), representing the species used in this study. (**B**) Sound recordings of the male calling songs with low (top) and high temporal resolution (below). (**C**) Extracellular recordings of the meso-Nv3A during fictive singing in the species studied. The wing-opener motoneuron activity is represented by open circles and the wing-closer motoneuron activity is represented by closed circles. The paired wing-opener and closer activity represents one pulse-period, i.e. the silent pulse-interval and the pulse. In each species the motor pattern of the fictive calling song reflects accurately the pattern of the natural calling song.

Figure 2. Structure of the abdominal ascending opener-interneuron A3-AO in cricket species.

(**A**) Morphology of A3-AO with cell body and dendrites in A3 and axonal projections in thoracic ganglia T2 and $T3_{A1/A2}$ (dorsal view). (**B**) Maximum intensity projections of confocal image stacks showing the fluorescence-labelled (Lucifer Yellow, green **[Bi]** and Alexa 568, red **[Bii]**) arborizations of the two pairs of bilateral symmetrical A3-AO in *T. commodus.* Both stainings reveal dye-coupling between the left and right neurons. The intracellular injection of the two dyes was performed in the same animal in different regions of the A3 ganglion. The merge **(Biii)** of the two projections shows a perfect correspondence between the two stainings. Arrows mark the cell bodies. Scale bars 150 μm. (**C**) In *T. oceanicus*, maximum intensity projections of confocal image stacks of staining a single interneuron with neurobiotin-avidinCy3 revealed the arborizations of two pairs of bilateral A3-AO interneurons. **(Ci)** In one animal two cell bodies occurred unilaterally on the left-hand side and one cell body on the right-hand side. **(Cii)** Another staining revealed two cell bodies unilaterally on the left-hand side. Arrows mark the cell bodies. Scale bars 150 μm.

Figure 3. Intracellularly recorded activity of A3-AO in the different cricket species.

(**A-E**) Activity of the A3-AO (top trace) and singing motor pattern (meso-Nv3A, lower trace). (**Ai-Ei**) The black dashed box shows the section highlighted at higher temporal resolution in Aii-Eii, the grey horizontal dashed line represents the resting membrane potential. (**Aii-Eii**) During fictive singing A3-AO depolarized and spiked in phase with wing-opener activity (open circles) and was hyperpolarized in phase with the wing-closer activity (closed circles). Arrows, indicate small spikes riding on a large excitatory post-synaptic potential (EPSP). The ramp depolarization is marked in blue in Aii and Bii.

Figure 4. Ramp depolarization and membrane potential changes in A3-AO.

(**A-E**) Intracellular recordings of the A3-AO show a gradual increase in the membrane potential above the resting potential (horizontal dashed line). This ramp depolarization (blue section) occurred at the start of singing activity before the generation of the first burst depolarization. A horizontal arrow marks the duration of the ramp and vertical stippled lines mark the points used to calculate the amplitude of the ramp, i.e. the resting membrane potential and the start of the burst depolarization. (**Ai-Ei**) The first two burst depolarizations of a singing

episode, with details of the membrane potential changes. The peak hyperpolarization is followed by a transition phase (H-to-T, horizontal dashed line), followed by a fast rise in membrane potential that triggers the first spike of the burst (T-to-S, vertical dashed line), as indicated by arrows.

Figure 5. Injection of depolarizing current pulses in A3-AO elicits singing activity.

Ai-Ei: In all species intracellular injection of +4 nA for 155 ms (red bar, top trace) elicited rhythmic A3-AO activity (middle trace) with depolarization–hyperpolarization cycles and the corresponding singing motor pattern (lower trace). (**Aii-Eii**) The response driven by the current pulse at a high temporal resolution. (**Aiii-Eiii) Probability distribution** of pulse periods, as calculated from the start of wing-closer bursts, see *inset* in *Aii*. Pulse periods induced by pharmacological brain stimulation are represented in blue and the ones induced by A3-AO current injection in orange, bins are 10 ms. Each distribution was sampled from 4 animals. For the brain stimulation and current injection, the number of pulse periods analyzed were: in *G. bimaculatus* 1138 and 1840; in *G. assimilis* 1459 and 1834; in *G. rubens* 1247 and 1508; in *T. commodus* 1816 and 1198 and *T.* oceanicus 1788 and 1891. Note, the outline of the background histogram (orange) is superimposed over the foreground histogram (blue) in order to make both histograms clear.

Figure 6. Stimulating A3-AO with long current pulses generates different phases of the song pattern in *Teleogryllus* species.

(Ai-Bi) Sustained intracellular injection of +3 nA for 3.4 s (red bar, top trace) elicited rhythmic A3-AO activity (middle trace) and rhythmic singing motor pattern (lower trace) until the current injection ceased. In *T. commodus*, three different types of membrane potential oscillations occurred during long A3-AO depolarization. The motor pattern started with a fast section composed of 3-6 pulses (1st Fast Section; median pulse period: 34.9 ms, IQR: 31.7 ms/37.6 ms), followed by a slow section with 5-10 pulses (Slow Section; median pulse period: 60.5 ms, IQR: 56.6 ms/64.3 ms), and a subsequent continuous fast section (2nd Fast Section; median pulse period: 41.3 ms, IQR: 38.3 ms/44.4 ms). In *T. oceanicus*, activity started with an unusually fast rhythm (Fast Section; median pulse period: 27.7 ms, IQR: 25.1 ms/30.5 ms), followed by a slower section (Slow Section; median pulse period: 63.4 ms, IQR: 57.4 ms/69.1 ms) and finally by section with an intermediate rhythm (Intermediate Section; median pulse period: 42.5 ms, IQR: 39.4 ms/46.3 ms). **(Aii-Bii)** Frequency distribution of pulse periods as calculated from the start of wing-closer bursts. The different phases of the singing episode are identified based on the pulse periods. Duration of pulse period (x-axis) plotted against the number of occurrences of each pulse period, bin width 10 ms. In both species, three sections could be identified based on the pulse period, which significantly differed between the sections (Kruskal-Wallis: $p<0.0001$; Dunn's multiple comparison test, $p<0.0001$; N=4, n=10 stimuli/animal).

Figure 7. Rhythmic *depolarization* of A3-AO determines temporal structure of singing episodes.

(**Ai-Ei**) Depolarization of A3-AO with current pulses of 4 nA (red bar, top trace) elicits rhythmic activity in the interneuron (middle trace) and corresponding fictive singing motor activity (lower trace). Different current durations were used for the different species, the A3-AO interneuron is only active for the duration of the current injection. In all five species the temporal structure of the singing activity is determined by the temporal pattern of the current-imposed A3-AO activity. In *G. rubens* and *T. oceanicus* motor activity in the Meso-Nv3A

(indicated by grey *) is not related to singing, it lacks rhythmicity, it is different in amplitude and the A3-AO is not active at the same time.

Figure 8. Depolarization of A3-AO resets the chirp pattern in *Gryllus* species.

(**Ai-Ci**) Reset of *Gryllus* chirp patterns by depolarizing current injection in A3-AO; 4 nA, 100 ms or 500 ms. Grey boxes indicate the chirp pattern before stimulation and the predicted subsequent timing. A3-AO stimulation causes shifts in the chirp activity relative to the expected timing. Note, concurrent to the current stimulation, a stimulus artifact occurs. (Aii-Cii) Phase-response diagrams for current pulses of 100 ms (grey circles) and 500 ms (black circles) show that the shift of the chirp pattern depends linearly on the stimulus phase and current duration, except for 100 ms current injection in *G. rubens*. Inset: T_{n-1} is the chirp period before stimulation; t is the time from the beginning of the chirp to the time of the current pulse; T_n is the chirp period after stimulation.

Figure 9. Post-inhibitory rebound in A3-AO.

(**Ai-Ei**) A hyperpolarization (-5 nA, 1s; blue bar; top trace) of the A3-AO (middle trace) was followed by a rebound depolarization and rhythmic membrane potential oscillations with burst spike activity, which elicited rhythmic wing-opener and wing-closer activity (lower trace). The latency of the rebound depolarization was measured from the end of the current pulse and the first spike of the following depolarization (horizontal arrow). The rebound depolarization amplitude was measured, for each depolarization, from the resting membrane potential and the peak of the depolarization (vertical arrows). (**Aii-Eii**) The latency of the rebound depolarization is plotted against different hyperpolarizing current amplitude steps from -0.5 nA to -10 nA. Latency was determined from the end of the current pulse to the first A3-AO spike elicited.

Table legends

Table 1. Song properties and fictive motor pattern in the cricket species studied.

Table 2. Properties of the A3-AO: Ramp depolarisation and membrane potential changes.

Table 3. Properties of the A3-AO: Spike and burst activity

Tables

Table 1. Song properties and fictive motor pattern in the cricket species studied.

Species (N song/fictive pattern)	Pulse Duration		Pulse Period		Number of Pulses		Song/phrase[3] Duration		Song/phrase[3] Period	
	Song (ms)	Fictive[1](ms)	Song (ms)	Fictive[2](ms)	Song	Fictive	Song	Fictive	Song	Fictive
G. bimaculatus (N=5/5)	18.6±3.2	20.9±2.9	38.2±3.2	43±3.6	3.8±0.5 pulses/chirp	4.5±1 pulses/chirp	130±24 ms	188±5 ms	408±51 ms	459±92 ms
G. assimilis (N=8/8)	8.1±1.3	8.5±2.5	16.7±1.5	23.8±5.4	6.3±1.1 pulses/chirp	6.8±1 pulses/chirp	102±14 ms	142±22 ms	1.5±0.4 s	1.1±0.4 s
G. rubens (N=8/8)	11.1±2.2	14.8±3	26.3±4	27.3±6.6	62±34 pulses/trill	44±19 pulses/trill	1.5±0.7 s	1.1±0.7 s	2±1 s	1.3±0.7 s
T. commodus (N=8/4)	Chirp 30.4±2.4 Trill: 22.4±2	Chirp: 21.8±5.5 Trill: 15.4±3.6	Chirp: 60.9±4.5 Trill: 33.9±1.9	Chirp: 71.1±11 Trill: 42.2±7.8	Chirp:.5±0.4 pulses/chirp Trill: 9±1.1 pulses/trill	Chirp: 9.1±2 pulses/chirp Trill: 10.3±6 pulses/trill	Chirp: 303±38 ms Trill: 1.4±0.5 s	Chirp: 600±22 ms Trill: 611±472 ms	2.2±1 s	4.2±1.7 s
T. oceanicus (N=8/4)	Trill: 29±4.3 Chirp: 23.6±4.2	Trill: 23.2±0.9 Chirp: 16.8±1.2	Trill: 62.5±7.7 Chirp: 39.6±5.1	Trill: 70.3±15 Chirp: 53.3±9.3	Trill: 5.5±0.5 pulses/trill Chirp: 2±0.1 pulses/chirp	Trill: 8.8±4.3 pulses/trill Chirp: 2±1.1 pulses/chirp	Trill: 313±49 ms Chirp: 1.5±0.5 s	Trill: 632±75 ms Chirp: 1.5±0.7 s	2±0.5 s	2.3±1.9 s

[1] time between the start of the wing-opener to the start of wing-closer motoneuron activity

[2] time between the start of two consecutive wing-closer motoneuron activity

[3]in species of the genus Teleogryllus, with complex songs, phrase corresponds to both sections of the song

Table 2. Properties of the A3-AO: Ramp depolarisation and membrane potential changes.

Species (N)	Start Ramp Depolarization (ms)	Amplitude Ramp Depolarization (mV)	H-to-T interval (ms)	T-to-S interval (ms)	Rate of membrane potential change (mV/ms)
G. bimaculatus (N=5; n=50 chirps)	42±6.4	6±0.5	17±6.7	4.1±1.7	4.3
G. assimilis (N=10; n=100 chirps)	40±7	4.3±1.3	9.1±0.6	1.9±0.5	7.6
G. rubens (N=10; n=70 trills)	21±2.1	2.9±0.4	12±3.3	4.7±2.3	2.3
T. commodus (N=4; n=40 chirps/trills)	Chirp:101±11 Trill:47±5.5	Chirp:4.1±2.2 Trill:4.7±1.4	Chirp:35±4 Trill:14±2.1	Chirp:7.5±0.5 Trill:4.5±1.2	Chirp:2.2 Trill:3
T. oceanicus (N=4; n=40 chirps/trills)	Trill:51±15 Chirp: Not analysed, chirp intervals < 100ms	Trill:2.8±0.1 Chirp: Not analysed, chirp intervals < 100 ms	Trill:35±4 Chirp:18±0.1	Trill:4.2±0.4 Chirp:3.8±0.2	Chirp:3.7 Trill:3.6

Table 3. Properties of the A3-AO: Spike and burst activity

Species	Spikes per pulse	Spike delay to wing opener-motoneurons (ms) $\bar{x} \pm SD$	Depolarizations Amplitude (mV)	Hyperpolarization Amplitude (mV)
G. bimaculatus (N=5)	4-6	10.4±1.2	17.5±2.1	9.2±2.5
G. assimilis (N=10)	3-6	8.9±1.2	1^{st}: 11±2.0 Middle: 14.9±4.6 Last: 10.4±3.1	1^{st}: 9.8±2.7 Middle: 7.5±1.4 Last: 11.7±3.1
G. rubens (N=10)	2-4	9.8±1.4	10.5±4.7	8.1±3.5
T. commodus (N=4)	Chirp: 3-7 Trill: 3-9	Chirp: 11.6±1.4 Trill: 11.2±1.3	Chirp: 16.4±4.1 Trill: 13.4±3.8	Chirp: 10.1±3.2 Trill: 6.5±2.5
T. oceanicus (N=4)	Trill: 4-6 Chirp: 2-5	Trill: 10.9±2.3 Chirp: 11.0±2.3	Trill: 15.9±5.2 Chirp: 13.6±4.2	Trill: 9.5±3.9 Chirp: 7.2±3.3

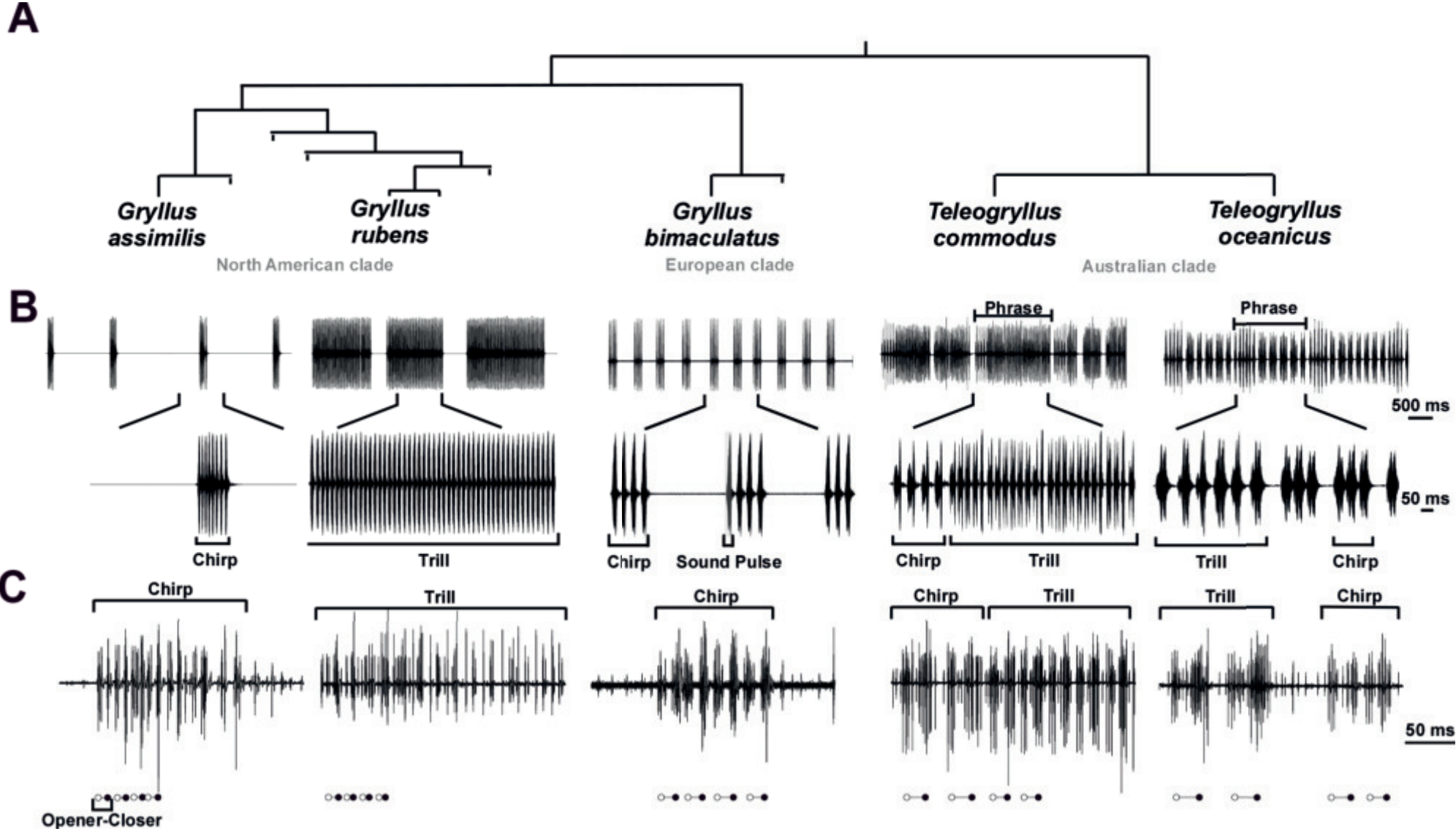
A
Gryllus assimilis
Gryllus rubens
Gryllus bimaculatus
Teleogryllus commodus
Teleogryllus oceanicus
North American clade
European clade
Australian clade
B
Phrase
Phrase
500 ms
50 ms
Chirp
Trill
Chirp
Sound Pulse
Chirp
Trill
Trill
Chirp
C
Chirp
Trill
Chirp
Chirp
Trill
Trill
Chirp
50 ms
Opener-Closer

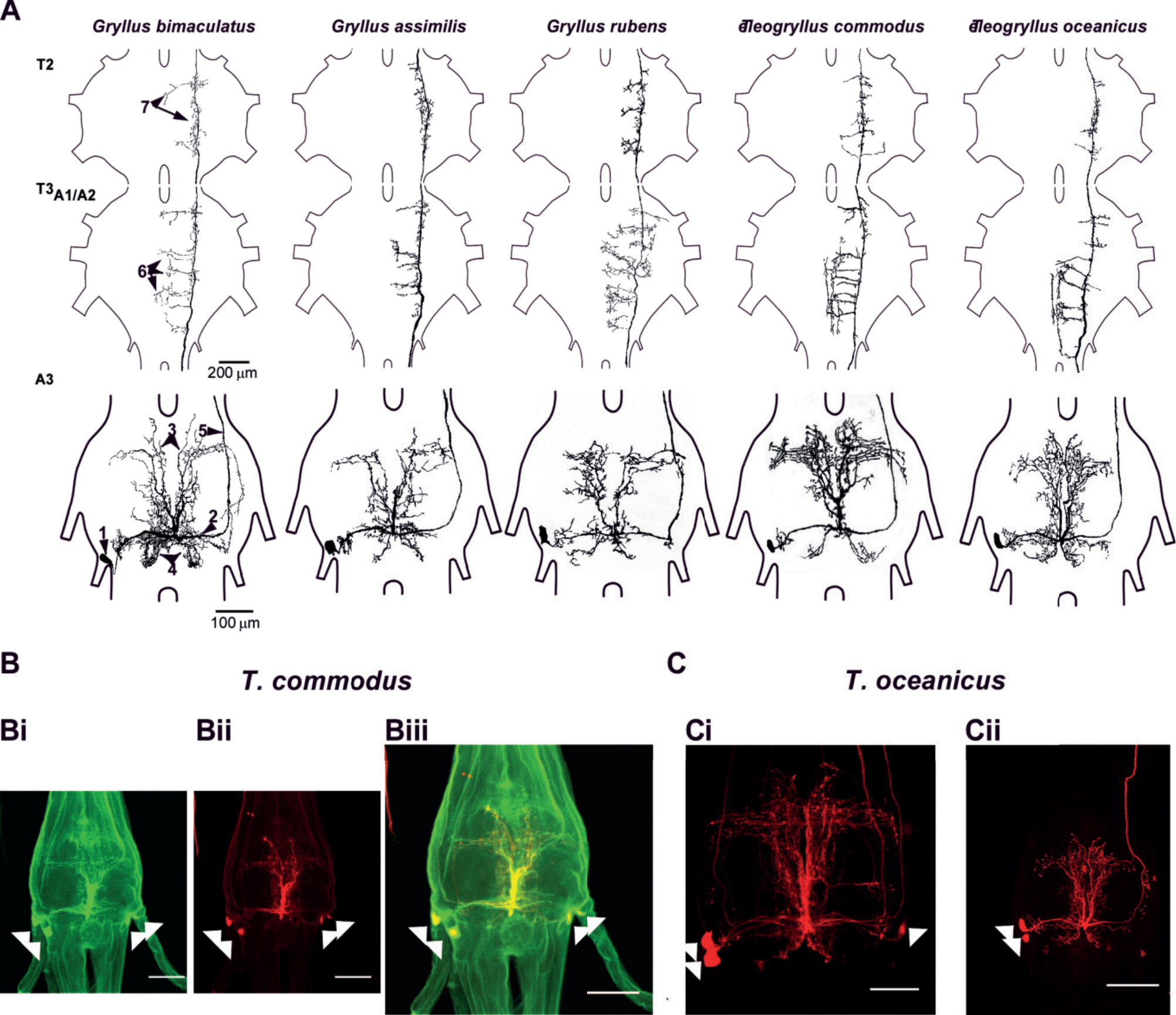
A
Gryllus bimaculatus
Gryllus assimilis
Gryllus rubens
Teleogryllus commodus
Teleogryllus oceanicus
T2
T3
A1/A2
A3
7
6
200 µm
3
5
2
1
4
100 µm
B
T. commodus
Bi
Bii
Biii
C
T. oceanicus
Ci
Cii

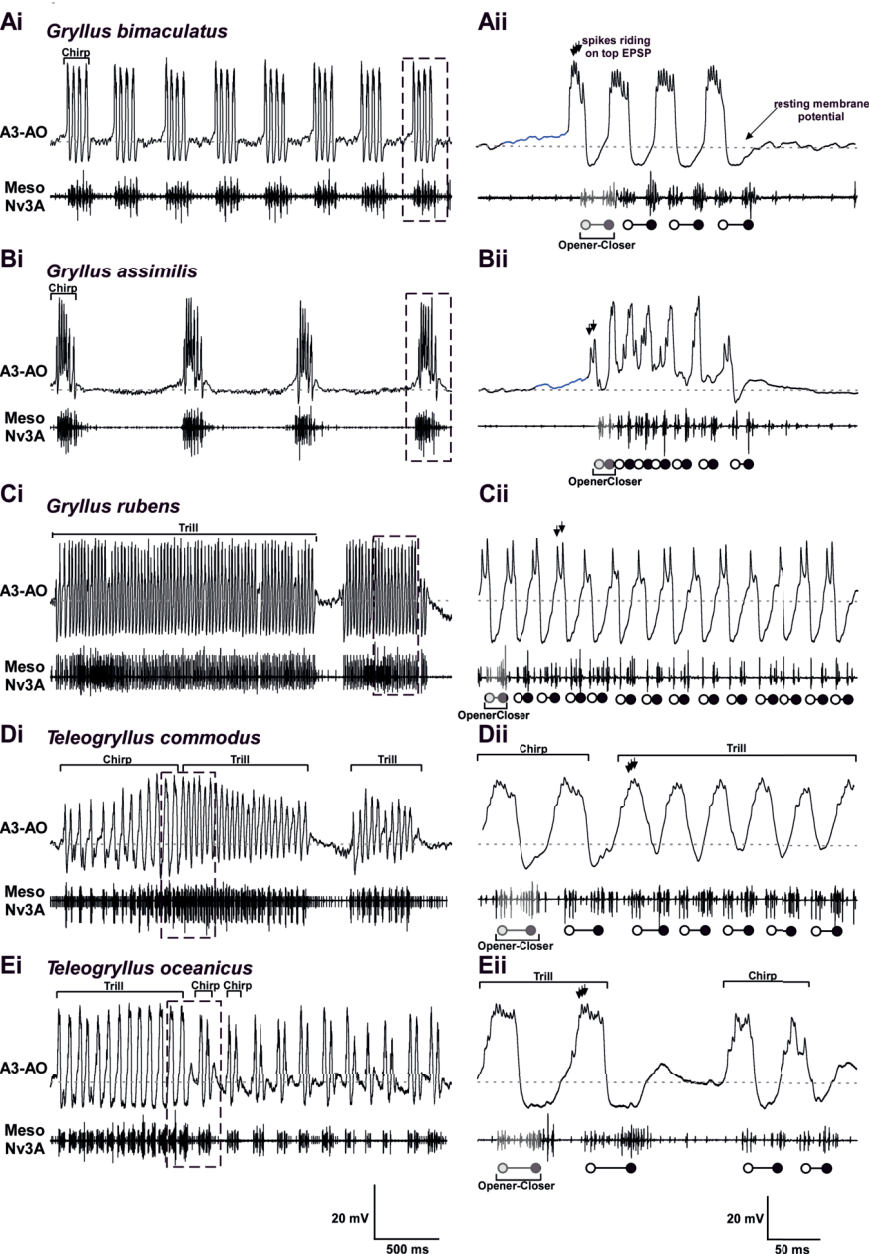
Ai
Gryllus bimaculatus
Chirp
A3-AO
Meso
Nv3A
Aii
spikes riding
on top EPSP
resting membrane
potential
Opener-Closer
Bi
Gryllus assimilis
Chirp
A3-AO
Meso
Nv3A
Bii
OpenerCloser
Ci
Gryllus rubens
Trill
A3-AO
Meso
Nv3A
Cii
OpenerCloser
Di
Teleogryllus commodus
Chirp
Trill
Trill
A3-AO
Meso
Nv3A
Dii
Chirp
Trill
Opener-Closer
Ei
Teleogryllus oceanicus
Trill
Chirp
Chirp
A3-AO
Meso
Nv3A
Eii
Trill
Chirp
Opener-Closer
20 mV
500 ms
20 mV
50 ms

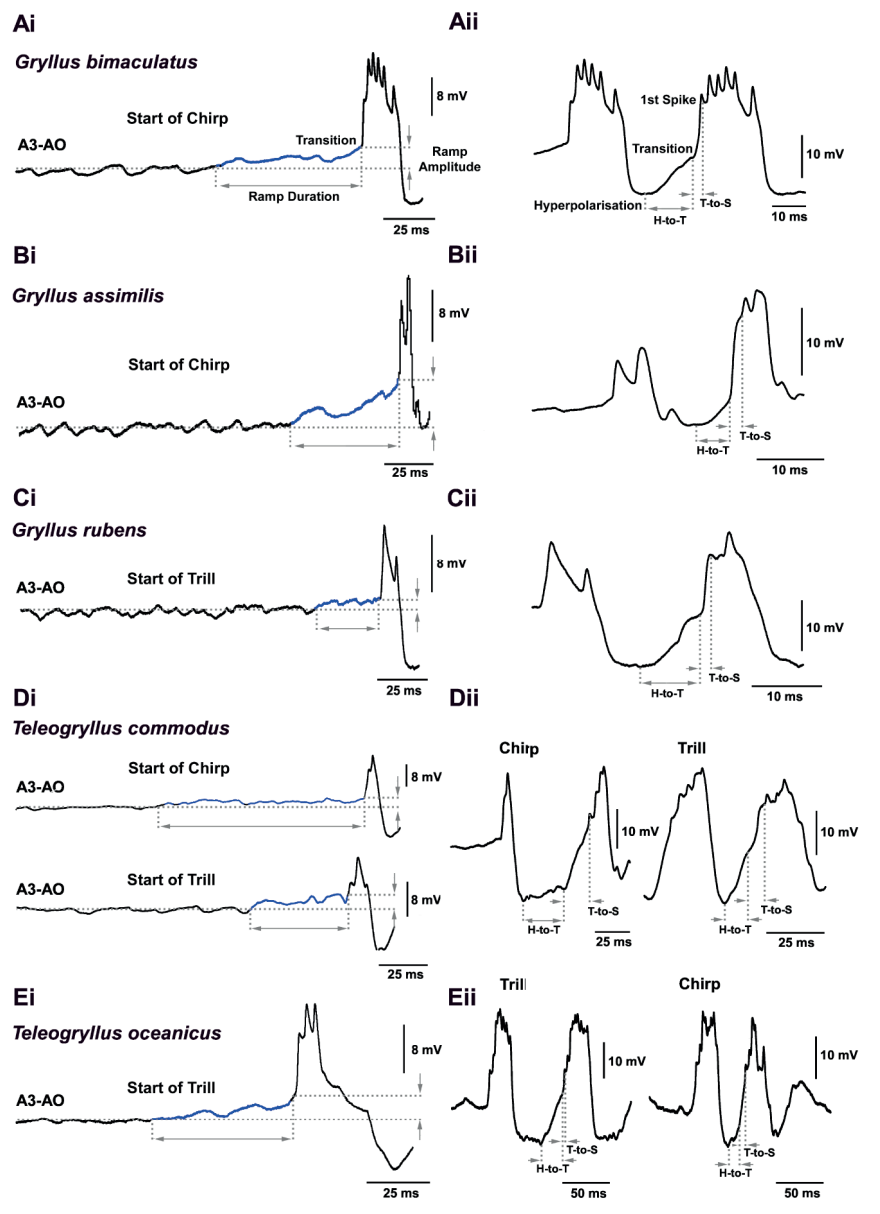
Ai
Gryllus bimaculatus
Start of Chirp
A3-AO
Transition
Ramp Amplitude
Ramp Duration
8 mV
25 ms
Aii
1st Spike
Transition
Hyperpolarisation
H-to-T
T-to-S
10 mV
10 ms
Bi
Gryllus assimilis
Start of Chirp
A3-AO
8 mV
25 ms
Bii
H-to-T
T-to-S
10 mV
10 ms
Ci
Gryllus rubens
Start of Trill
A3-AO
8 mv
25 ms
Cii
H-to-T
T-to-S
10 mV
10 ms
Di
Teleogryllus commodus
Start of Chirp
A3-AO
Start of Trill
A3-AO
8 mV
25 ms
Dii
Chirp
Trill
H-to-T
T-to-S
10 mV
25 ms
Ei
Teleogryllus oceanicus
Start of Trill
A3-AO
8 mV
25 ms
Eii
Trill
Chirp
H-to-T
T-to-S
10 mV
50 ms

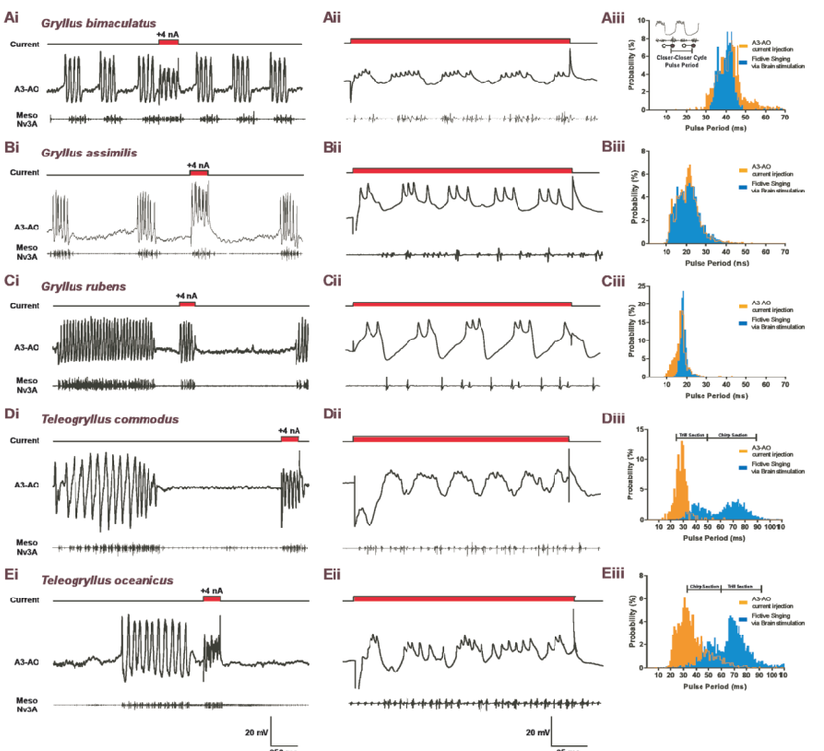
Ai
Gryllus bimaculatus
+4 nA
Current
A3-AO
Meso
N∨3A
Aii
Aiii
Closed-Closed Cycle
Pulse Period
A3-AO
current injection
Fictive Singing
via Brain-stimulation
Probability (%)
Pulse Period (ms)
Bi
Gryllus assimilis
Bii
Biii
Ci
Gryllus rubens
Cii
Ciii
Di
Teleogryllus commodus
Dii
Diii
Trill Section
Chirp Section
Ei
Teleogryllus oceanicus
Eii
Eiii
20 mV
250 ms
20 mV
25 ms

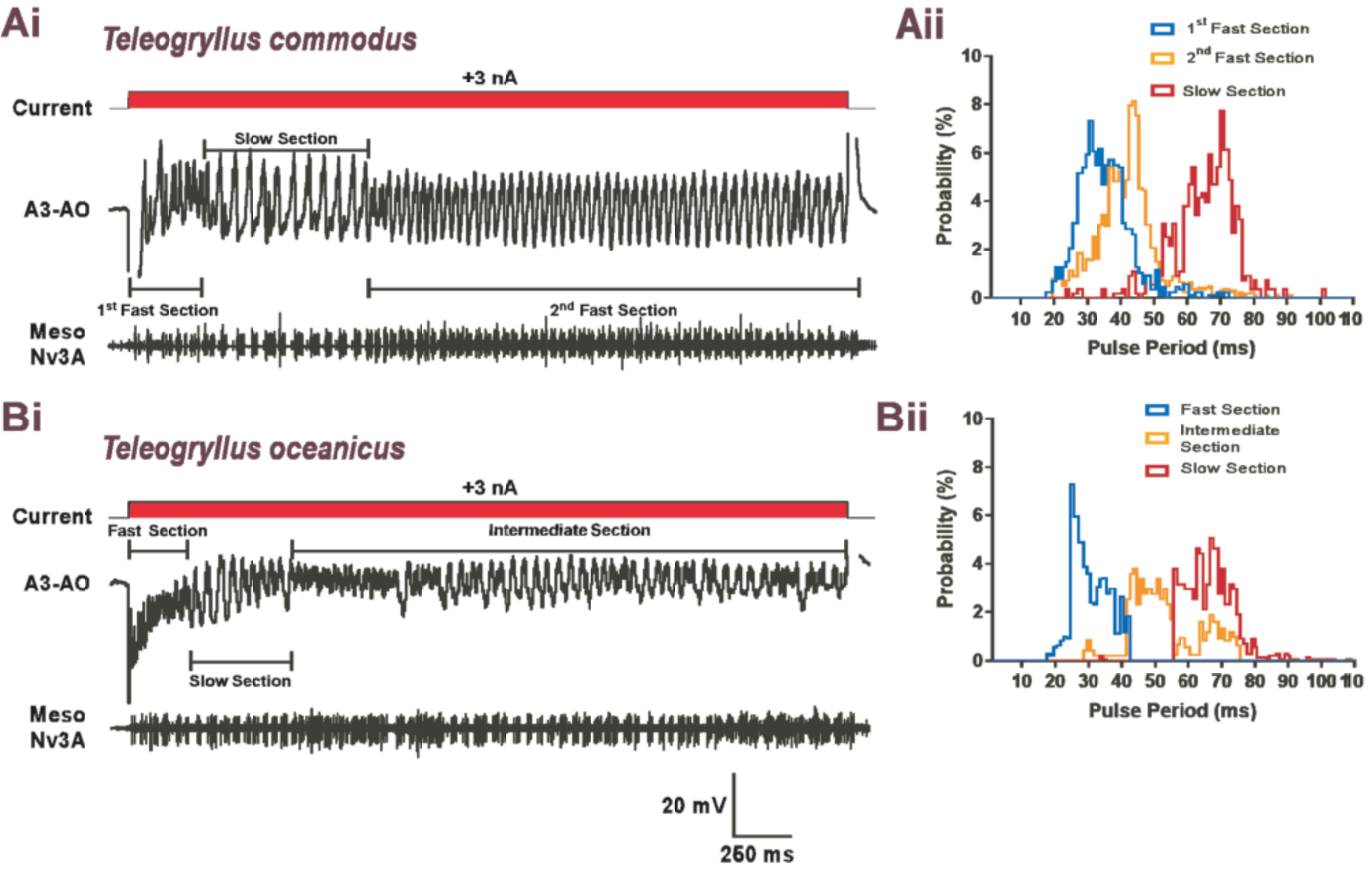
Ai
Teleogryllus commodus
+3 nA
Current
Slow Section
A3-AO
1st Fast Section
2nd Fast Section
Meso
Nv3A
Aii
1st Fast Section
2nd Fast Section
Slow Section
Probability (%)
Pulse Period (ms)
Bi
Teleogryllus oceanicus
+3 nA
Current
Fast Section
Intermediate Section
A3-AO
Slow Section
Meso
Nv3A
20 mV
250 ms
Bii
Fast Section
Intermediate Section
Slow Section
Probability (%)
Pulse Period (ms)

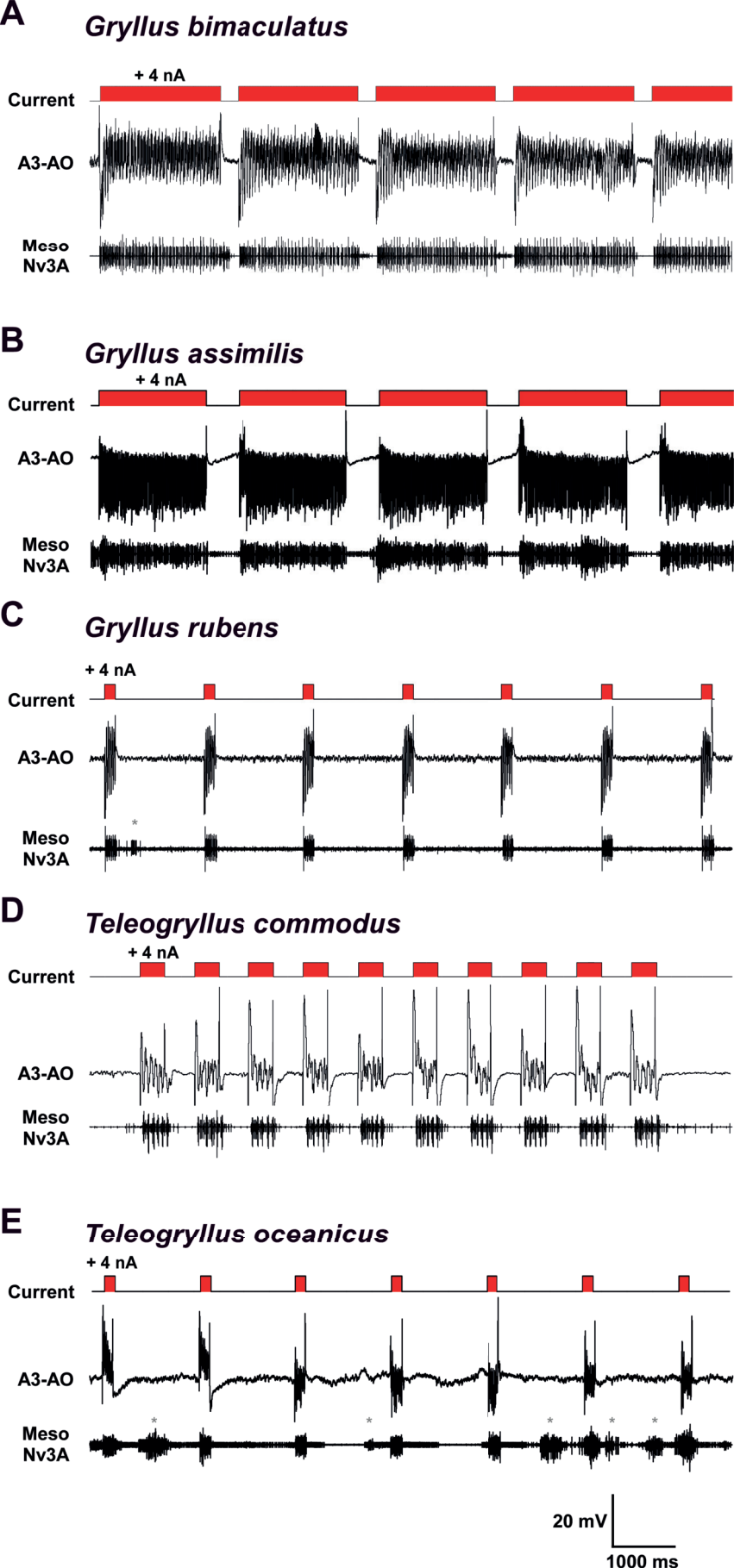
A
Gryllus bimaculatus
+ 4 nA
Current
A3-AO
Meso
Nv3A
B
Gryllus assimilis
+ 4 nA
Current
A3-AO
Meso
Nv3A
C
Gryllus rubens
+ 4 nA
Current
A3-AO
Meso
Nv3A
D
Teleogryllus commodus
+ 4 nA
Current
A3-AO
Meso
Nv3A
E
Teleogryllus oceanicus
+ 4 nA
Current
A3-AO
Meso
Nv3A
20 mV
1000 ms

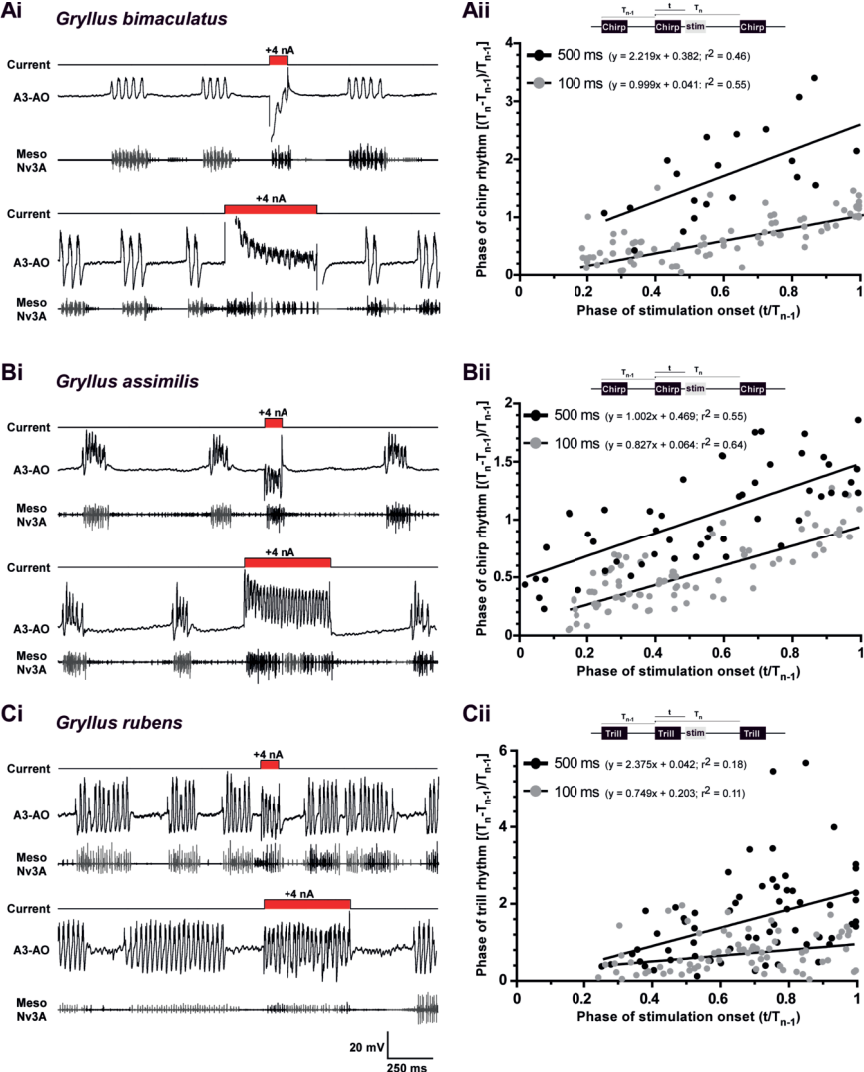
Ai
Gryllus bimaculatus
+4 nA
Current
A3-AO
Meso Nv3A
Aii
Chirp
Chirp-stim
500 ms (y = 2.219x + 0.382; r2 = 0.46)
100 ms (y = 0.999x + 0.041; r2 = 0.55)
Phase of chirp rhythm [(Tn-Tn-1)/Tn-1]
Phase of stimulation onset (t/Tn-1)
Bi
Gryllus assimilis
Bii
500 ms (y = 1.002x + 0.469; r2 = 0.55)
100 ms (y = 0.827x + 0.064; r2 = 0.64)
Ci
Gryllus rubens
Cii
Trill
Trill-stim
500 ms (y = 2.375x + 0.042; r2 = 0.18)
100 ms (y = 0.749x + 0.203; r2 = 0.11)
Phase of trill rhythm [(Tn-Tn-1)/Tn-1]
20 mV
250 ms

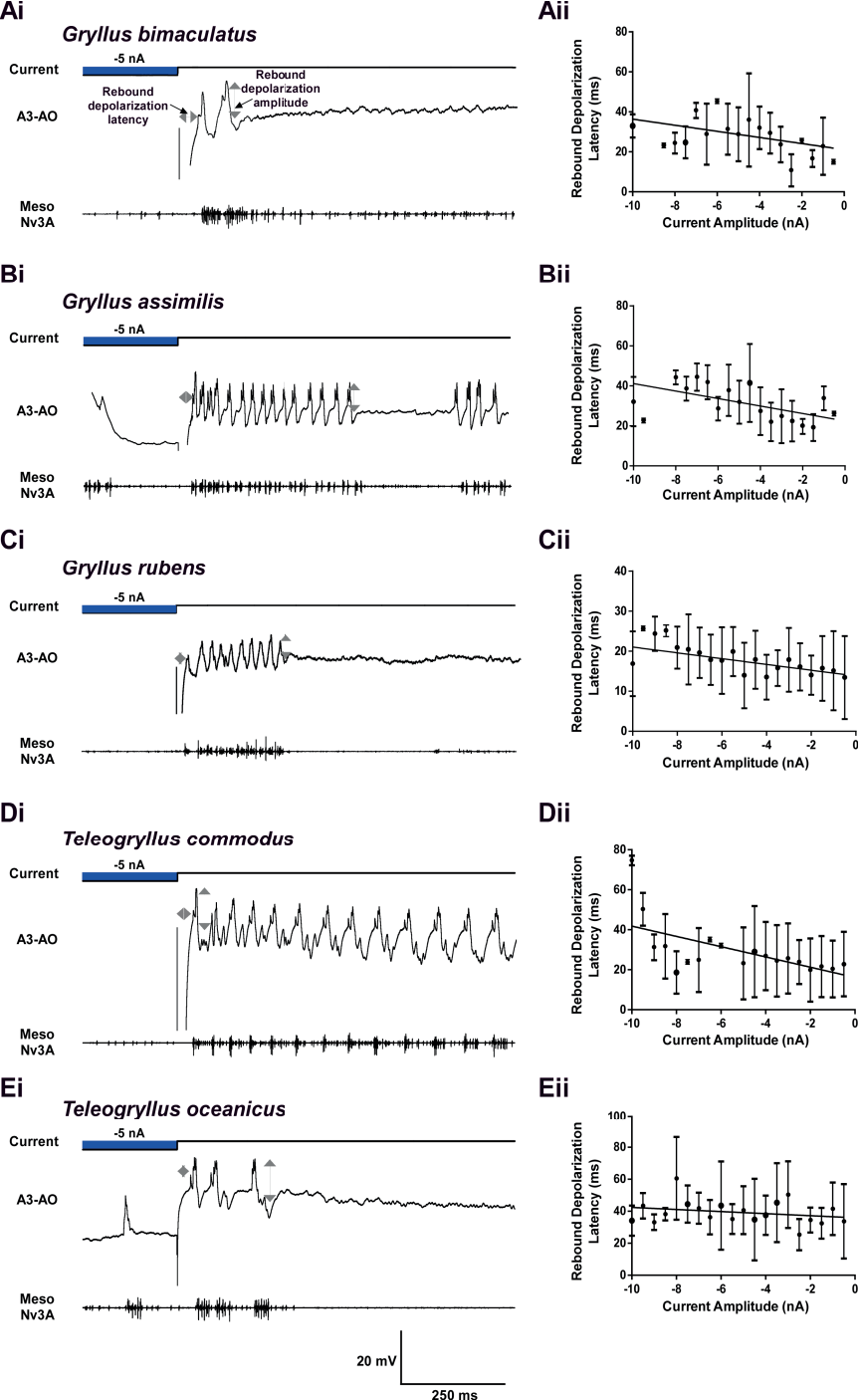
Ai
Gryllus bimaculatus
-5 nA
Current
A3-AO
Meso Nv3A
Rebound depolarization latency
Rebound depolarization amplitude
Aii
Rebound Depolarization Latency (ms)
Current Amplitude (nA)
Bi
Gryllus assimilis
Bii
Ci
Gryllus rubens
Cii
Di
Teleogryllus commodus
Dii
Ei
Teleogryllus oceanicus
Eii
20 mV
250 ms